IPPP/19/94, LAPTH-051/19

Determining the lifetime of long-lived particles at the LHC

Shankha Banerjee[1], **Biplob Bhattacherjee**[2], **Andreas Goudelis**[3], **Björn Herrmann**[4], **Dipan Sengupta**[5], **Rhitaja Sengupta**[2]

[1] *Institute for Particle Physics Phenomenology, Department of Physics, Durham University, Durham DH1 3LE, United Kingdom*

[2] *Centre for High Energy Physics, Indian Institute of Science, Bangalore 560012, India*

[3] *Laboratoire de Physique de Clermont (UMR 6533), CNRS/IN2P3, Univ. Clermont Auvergne, 4 Av. Blaise Pascal, F-63178 Aubière Cedex, France*

[4] *Univ. Grenoble Alpes, Univ. Savoie Mont Blanc, CNRS, LAPTh, F-74000 Annecy, France*

[5] *Department of Physics and Astronomy, University of California San Diego, 9500 Gilman Drive, La Jolla, California, USA*

E-mail: shankha.banerjee@durham.ac.uk, biplob@iisc.ac.in, andreas.goudelis@clermont.in2p3.fr, herrmann@lapth.cnrs.fr, disengupta@physics.ucsd.edu, rhitaja@iisc.ac.in

Abstract: We examine the capacity of the Large Hadron Collider to determine the mean proper lifetime of long-lived particles assuming different decay final states. We employ model-dependent and model-independent methods in order to reconstruct the proper lifetime of neutral long-lived particles decaying into displaced leptons or jets, potentially accompanied by missing energy, as well as charged long-lived particles decaying into leptons and missing energy. After a generic discussion, we illustrate and discuss these methods using several new physics models. We conclude that the lifetime can indeed be reconstructed in many concrete cases. Finally, we discuss to which extent including timing information can improve such an analysis.

Contents

1 Introduction

The lack of observation of new physics at the Large Hadron Collider (LHC) has prompted a re-evaluation of the strategies aiming to probe signals of physics beyond the standard model (BSM). Initial expectations had been that new physics would

reveal itself in prompt searches involving leptons, jets, and missing energy, or, eventually, in the form of exotic resonances. However, no smoking gun signal has appeared in such searches so far. It is, therefore, only reasonable to entertain the possibility that new physics may manifest itself in unexpected ways, in the form of non-standard signatures. Although such a *terra incognita* can be daunting to explore, we can appeal to well-motivated theoretical scenarios for guidance. An attractive possibility is that some of the produced particles are long-lived, *i.e.* that the secondary vertices through which they decay are macroscopically displaced with respect to the primary interaction point at which they are produced. Such signatures appear in a large variety of new physics frameworks such as Supersymmetry [1–14], Twin Higgs models [15], or Hidden Valley models [16–18], as well as in frameworks including dark matter [19–25] or baryogenesis [26].

Searches for long-lived particles (LLPs) are already being pursued at ATLAS and CMS in LHC, see, *e.g.*, Refs. [27–37] and will be one of the primary focus of new physics searches at the LHC in the coming years. For an overview of recent LLP searches, we refer the reader to Ref. [38] and references therein. In addition to the multi-purpose experiments ATLAS and CMS, dedicated detectors like FASER [39] and MATHUSLA [40] have been proposed to probe long-lived particles [41]. The range of new physics scenarios that such detectors can explore is both vast and very well-motivated [42, 43]. Moreover, these proposals aim at filling in a "lifetime gap" between prompt collider searches and cosmological constraints such as Big Bang Nucleosynthesis (BBN), which is typically sensitive to lifetimes of the order of 0.1 s or longer [44].

From an experimental perspective, the definition of what precisely is a long-lived particle depends on each detector and its ability to measure a vertex location with a certain degree of accuracy. As the LHC enters a new phase, hardware and technological upgrades make it more efficient in pinning down this location with greater accuracy.

In this work we will consider LLPs as states with a proper lifetime greater than about 100 ps, the lower limit originating from the timing resolution. Such lifetimes can be induced either by rather small couplings or in specific kinematic configurations involving small mass splittings between the particles participating in the process or large propagator masses. Regardless of the underlying physics, LLPs introduce significant additional complications for experimental searches as compared to promptly produced particles. If the LLP is heavy and charged, it will leave a distinct track in the detector, making detection easier, while neutral LLPs are more difficult to detect.

In this paper, we place ourselves in the *hopeful* scenario that Long-Lived Particles are observed at the Large Hadron Collider and we examine its capacity to reconstruct the LLP lifetime. Extracting such information can not only provide crucial information in order to, at least partly, reconstruct features of the underlying microscopic

model, notably the coupling strength between the LLP and its decay products, but may also lead to the establishment of more unexpected connections between LHC observations and, *e.g.*, cosmology, for an example see Ref. [23]. Motivated by our simple analysis presented in Ref. [45], we explore several ways to estimate the lifetimes of different kinds of LLPs with multifarious decay modes. To the best of our knowledge, only few of such studies have appeared in the literature, focusing on different LLP decay channels [46, 47]. A way to estimate the lifetimes of Charged Massive Stopped Particles (CHAMPs) has been studied in Ref. [46]. In the analysis that follows, at various stages, we will allow for some leeway, in terms of the known quantities available to us, as well as potentially speculate on some uncertainties that will only be precisely estimated once the LHC run-3 starts.

We present ways to estimate the lifetime of LLPs considering various decay channels into different final states. We start with the simplest case of displaced leptons, continue with displaced jets and, eventually, study LLP decays involving invisible particles. Most of the analyses presented here can be applied to numerous LLP models involving such final states and also in several future colliders. Finally, we also study the prospect of the proposed MIP Timing Detector (MTD) in improving the determination of the LLP lifetime.

The paper is organised as follows: In Sec. 2, we start by recalling basic formulae related to the LLP lifetime and discuss why we restrict ourselves to LLP decays within the tracker. In Sec. 3, we discuss why the LLP lifetime cannot be reconstructed through a naive exponential fit, we propose alternative approaches and we study how these can be used to estimate the lifetime for different LLP decay modes. Sec. 4 is dedicated to a discussion of the MTD and how adding the timing information can improve the situation, not only concerning the lifetime estimation but also in order to identify the model by reconstructing the mass of the LLP in cases where the LLP decays involve invisible particles. Our conclusions are presented in Sec. 5.

2 Long-lived particle lifetime reconstruction

We start this section by reviewing some relations related to the lifetime of long-lived particles (LLPs).

2.1 Kinematics of LLPs

In the laboratory frame, the decay length of a particle with proper decay time τ (as measured in its own rest frame) is given by

$$d \;=\; \beta\gamma c\tau\,, \tag{2.1}$$

where $\gamma = E/m = (1-\beta^2)^{-1/2}$ is the relativistic factor with $\beta = v/c = |\vec{p}|/E$, v is the velocity of the decaying particle and c denotes the speed of light. The decay

probability of such particles follows the same distribution as the one encountered in radioactive decays. If we consider the production of a number N_0 of such unstable particles with mean proper lifetime τ, the expected number of surviving particles $N(t)$ evolves as a function of time t through the usual exponentially decreasing distribution

$$N(t) \;=\; N_0\, e^{-t/\tau}\,. \tag{2.2}$$

By measuring the decay length d_i of each event, together with the corresponding kinematical factor β_i, we can deduce the proper decay time associated to the event. Ideally, it is possible to infer the values of N_0 and τ by performing an exponential fit of the sample data, provided that enough statistics is available. If the proper decay length is large, the number of LLP decays within the detector volume will be very small, and therefore we will require a large enough statistical sample to perform a faithful fit.

We note that the geometrical acceptance probability for an LLP with a decay length d as it traverses the detector is given by

$$P_{\rm dec} \;=\; \frac{1}{4\pi}\int_{\Delta\Omega} {\rm d}\Omega \int_{L_1}^{L_2} {\rm d}L\; \frac{1}{d} e^{-L/d}\,, \tag{2.3}$$

where L_1 and L_2 are the distances between the interaction point and the point where the LLP respectively enters and exits the decay volume, and $\Delta\Omega$ is the geometric cross section of the active detector volume [43]. Thus we clearly see that while the LHC can be sensitive to decays occurring within a certain displacement, the probability decreases if the displacement length is significant[1].

At a hadron collider like the LHC, transverse momentum p_T and the rapidity separation of particles $\Delta\eta$ are two of the most important observables as they are longitudinal boost invariant. Thus, we define a transverse decay length,

$$d_T \;=\; \beta_T \gamma c\tau\,, \tag{2.4}$$

where $\beta_T = \frac{p_T}{m}$, is the transverse boost of the LLP. We will implement basic event selection criteria on the events including the transverse momentum and the rapidity, and therefore d_T and β_T will be useful variables for this analysis. Along with the transverse decay length d_T, the longitudinal displacement of the LLP, d_z, along the beamline will be a kinematic variable of interest to us.

In the following, we will consider the production of a variety of long-lived particles, hereafter denoted by X, with different decay modes. The long-lived particle can be charged or neutral and therefore its identification efficiency depends on the tracker and the energy deposition in the detector, among various other factors.

[1]Next generation dedicated LLP detectors like MATHUSLA[40] and FASER[39] can therefore provide further coverage of the associated parameter space.

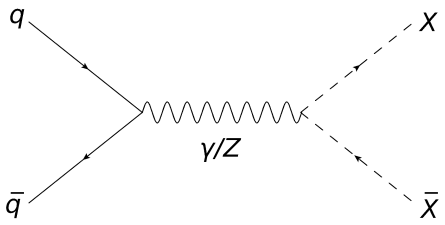

Figure 1: Quark-initiated s-channel pair production of scalar LLPs

2.2 Restricting to decays within tracker

In order to estimate the lifetime of the long-lived particle X, in the following we will restrict ourselves to decays occurring inside the tracker region of the detector. This not only allows access to the position of the secondary vertex (SV), but also helps in reconstructing the charged decay products of X as well as in the measurement of the boost factor $\beta\gamma$. However, this restriction will limit the number of observed LLP decays, especially in the case of particles characterised by longer lifetimes leading to decays outside the tracker region. In this section we quantify the fraction of decays we can expect within the tracker for given ranges of LLP masses and lifetimes.

Consider the production of a pair of long-lived particles at the LHC, $pp \to XX$, and their subsequent decays into Standard Model particles. Since the boost factor $\beta\gamma$ of the particles X depends on their production mode, for illustration we focus on a supersymmetric (SUSY) model containing a LLE-type R-parity violating (RPV) coupling, for a review *cf e.g.* [48]. In this model a pair of sneutrino LLPs is produced through a quark-initiated s-channel process as in Figure 1 and decays into two electron pairs, with a mean proper lifetime that is controlled by the LLP mass and the magnitude of the RPV coupling. Events have been simulated using `PYTHIA6` [49].

In Figure 2 we show the variation of the fraction of LLP decays as a function of the LLP mass and proper decay length. We focus on two intervals for the decay length, namely a decay within 30 cm (left panel) or between 30 cm and 100 cm (right panel) from the beam line. The former corresponds to the transverse dimension of the ATLAS Pixel detector and the latter is the rest of the tracker region [50]. Similarly, the CMS Pixel detector extends radially up to ~ 16 cm and the full tracker extends up to $\sim$129 cm.

For particles with masses in the TeV range, we observe that even for proper lifetimes of the order of a few meters, about 40% of the decays are expected to take place within 30 cm from the beam line, *i.e.* within the silicon detector. For lighter particles having masses around 10 GeV, this fraction turns to 20%, provided the proper lifetime is $c\tau \lesssim 1$ m. For even lighter particles, the sensitivity will be reduced, since they may have larger boost factors and consequently decay much later. Considering radial distances between 30 cm and 100 cm from the beam line,

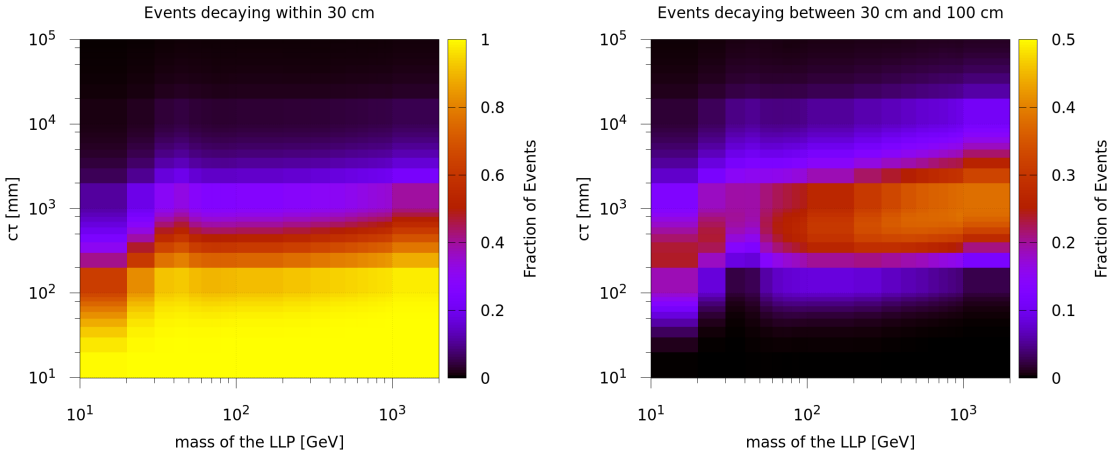

Figure 2: Dependence of the fraction of LLPs on the mass and proper decay length ($c\tau$) of the LLP considering decays within 30 cm (left) and (right) between 30 cm and 100 cm (right) from the beam line.

we find that we can expect at least 10% decays within this region for a mass of about ~ 1 TeV and a mean proper lifetime of $c\tau \sim 10\,\text{m}$. The same fraction of decays is expected for a particle mass of about 10 GeV and a proper lifetime of $c\tau \sim 1\,\text{m}$.

The small increase in the fraction of decays within 30 cm and a subsequent dip in the corresponding fraction in the region between 30 cm and 100 cm, for LLP masses around $40 - 50$ GeV is due to the presence of the Z-pole in the LLP pair-production cross-section. At these mass values, the LLPs will preferentially be produced by the decay of an on-shell Z-boson and hence they will have very little boost and smaller decay lengths.

We also notice that in the right panel plot of Fig. 2, a red region is sandwiched between two purple regions, *i.e.*, the decay fraction in this region first rises and then falls again. This is because as the lifetime increases up to a particular value ($c\tau \sim$ few 100 mm), we expect the decay fraction in this region to increase. However, when the lifetime becomes much higher, the decay length distribution becomes flatter and hence, the chances of the LLP to decay in regions of the detector outside the tracker also increase, making the decay fraction in this region decrease.

In summary, we find that for a wide range of proper decay length values $c\tau$, the probability of the LLP to decay within a distance of 30 cm from the beam line is substantial. In the following, we will therefore restrict ourselves to decays taking place within this radius, *i.e.* within the ATLAS Pixel detector, where the measurements of the secondary vertex position and the boost factor $\beta\gamma$ of LLP are the most precise.

3 Lifetime reconstruction for different LLP decay modes

After the previous preliminary remarks, let us now turn to our analysis. We will study to which extent the lifetime of a long-lived particle (LLP) can be reconstructed considering the following four decay scenarios:

- Displaced leptons: In this case we will assume a neutral LLP decaying into a pair of leptons. We will generate our Monte Carlo data set using a supersymmetric model containing a LLE-type R-parity violating coupling. In this model the sneutrino is the LLP and it decays into two electrons.

- Displaced jets: Here we will consider a neutral LLP decaying into two jets. In this analysis, we will again use the R-parity-violating supersymmetric framework, but with a LQD-type coupling inducing the decay of a long-lived sneutrino into a jet pair.

- Displaced leptons with missing transverse energy ($\not{E}_{\mathrm{T}}$): We will assume a neutral LLP decaying into a pair of leptons along with an invisible particle. Here we will employ a minimal Gauge-Mediated Supersymmetry Breaking (GMSB) model in which a long-lived lightest neutralino decays into a Z and a nearly massless gravitino. We will also discuss the feasibility of estimating the lifetime in a scenario with a heavier invisible particle in Section 4.1.2.

- Kinked (or disappearing) tracks: As a final case we will consider a charged LLP decaying into a lepton along with an invisible particle. The model that we will use for this analysis is again LLE-type RPV SUSY, with a slepton LLP decaying into a charged lepton and a neutrino.

In all the cases, the decay of the LLP to the respective final states is considered to have 100% branching. As a first approximation, we will ignore initial and final state radiation (ISR and FSR), multi-parton interactions (MPI), and smearing effects. Subsequently, we will also lift this approximation in order to quantify the impact of these effects on the LLP lifetime reconstruction.

Let us also note that this choice of models should not be taken to reflect any theoretical prejudice. They have been chosen simply for convenience, as they are already incorporated in the `PYTHIA6` framework and they can give rise to the experimental signatures that we will be studying in what follows. In the same spirit, we will not be concerned with the phenomenological viability of these models with regards to the full set of constraints that could be envisaged. Put simply, for the purposes of this work these models should be viewed as toy models. We must stress here that the aforementioned choices of models are only for simulation purposes. Any model giving rise to such production modes will exhibit the results discussed below. The results are general and hold for most models exhibiting the respective

topologies. Also, these analyses can be extended to any future collider with the only change being the modification in the kinematic cuts due to the different detector dimensions.

3.1 Displaced leptons

We start with the experimentally simplest case in which a long-lived particle X decays into two leptons within the inner tracker of ATLAS. In this case, the position of the secondary vertex can be identified precisely by observing the lepton tracks in the tracker [2]. In general, the larger the number of tracks, the greater is the efficiency of reconstructing the secondary vertex, *cf* Ref. [52]. The position of the secondary vertex for a pair of displaced leptons can be reconstructed with a precision of few ($\mathcal{O}(10)$ μm) in the transverse direction if the decay occurs towards the inner tracker region, and becomes more uncertain for longer transverse displacements, *cf* Refs. [38, 52]. The mass of the decaying particle X can be inferred from the dilepton invariant mass distribution. Finally, the boost factor of the decaying particle X can be determined as $(\beta\gamma)_{\rm LLP} = p/m$, where p and m are the absolute momentum and the invariant mass of the dilepton system, respectively. We present our analyses assuming two displaced electrons in the final state. In the case of muons, we need not restrict to the inner tracker and can rather consider decays up to the muon spectrometer [53]. In this case, we could also use the muon tracks in the muon spectrometer to reconstruct the secondary vertex as well as the four-momentum of the LLP.

3.1.1 Lessons from a naive exponential fit

Let us first attempt to reconstruct the LLP lifetime through a simple exponential fit [3]. We will see that experimental cuts introduce a bias on the sample and, hence, hamper the lifetime estimation. Solutions to this issue will be suggested in the following Section 3.1.2 and further elaborated upon in the subsequent Sections.

For this introductory exercise, we consider an ideal situation in which initial and final state radiation as well as smearing effects are absent, and the four-momenta of the long-lived particles X can be measured with infinite precision. We generate our data sample of parton-level events, $pp \to XX$, using `PYTHIA 6` for different masses and lifetimes of the particle X. Note that the $\beta\gamma$ distribution of the LLPs will vary depending on their production mode and is, therefore, a model-dependent quantity.

[2] Experimentally, the procedure to reconstruct a secondary vertex is generally done in two steps as detailed in [51]. The efficiency depends on the process/model in question, and on the associated number of charged particles/tracks that can be reconstructed first at the truth level and then at the detector level. The final efficiency can vary between as much as 100% for models with a large number of tracks to about 20% for models with leptons and missing energy.

[3] Note that part of this discussion has already been presented in Ref. [45]. In order to keep the presentation self-contained, we recapitulate the procedure here and expand upon it wherever necessary.

Following standard LHC guidelines, we demand that both the electrons coming from the decay of the long-lived particle X have transverse momentum $p_T > 20$ GeV and pseudorapidity $|\eta| < 2.4$. The samples with only the p_T and η cuts applied will be referred to as "basic cuts" (BC). Since the reconstruction of the secondary vertex becomes more difficult and less precise as the latter approaches the outer surface of the tracker, we impose an additional condition on the displacement of the secondary vertex with respect to the interaction point. We restrict ourselves to events for which the transverse decay length d_T of X lies within the Pixel Detector of the ATLAS tracker (which extends out to 30 cm in the radial direction and the displacement $|d_z|$ in the longitudinal direction is within 300 cm which corresponds to the half-length of the ATLAS tracker. The samples with these additional cuts on the decay length along with the basic cuts applied will be hereafter referred to as "extra cuts" (EC). All used cuts can be summarized as follows:

(BC) $p_T > 20$ GeV and $|\eta| < 2.4$ for both electrons,

(EC) 0.1 cm $< d_T <$ 30 cm and $d_z <$ 300 cm for displacement of secondary vertex, in addition to (BC).

In Figure 3 we show the impact of these cuts on the decay length $d = \beta\gamma c\tau$, proper lifetime τ and $\beta\gamma$ distributions (top-left, top-right and bottom-left panels respectively), when applied individually as well as all combined. We observe that the pseudorapidity cut on the electrons introduces a bias on the $\beta\gamma$ distribution towards smaller values. This is explained by the fact that the $|\eta|$ cut restricts the z-component of the momenta of the electrons to low values and hence rejects events characterised by high values of $\beta\gamma = p/m = \sqrt{p_x^2 + p_y^2 + p_z^2}/m$. On the other hand, we see that the cuts on the p_T of the electrons and on the transverse decay length of X affect the $\beta\gamma$ distribution only slightly.

For the decay length d, we observe that this distribution is mostly affected by the cuts on the transverse decay length of X, pushing the spectrum towards lower values of d. Similarly, these cuts also shift the proper lifetime τ distribution towards lower values, hence, biasing our samples in favour of events characterised by smaller proper decay lengths. This implies that the observed distribution is overall skewed with respect to the underlying one, and our estimate for the lifetime will also be biased towards smaller values.

Note that for the High-Luminosity (HL) LHC upgrade, the pseudorapidity coverage will extend up to about $|\eta| \lesssim 4.0$ [54]. In the bottom-right panel of Figure 3, we also show the effect of such a looser cut on the $\beta\gamma$ distribution (bottom-right panel). We observe that in this case the $\beta\gamma$ distribution is affected substantially less, implying that the HL-LHC upgrade may perform better in estimating the LLP lifetime. We will come back to this point later on.

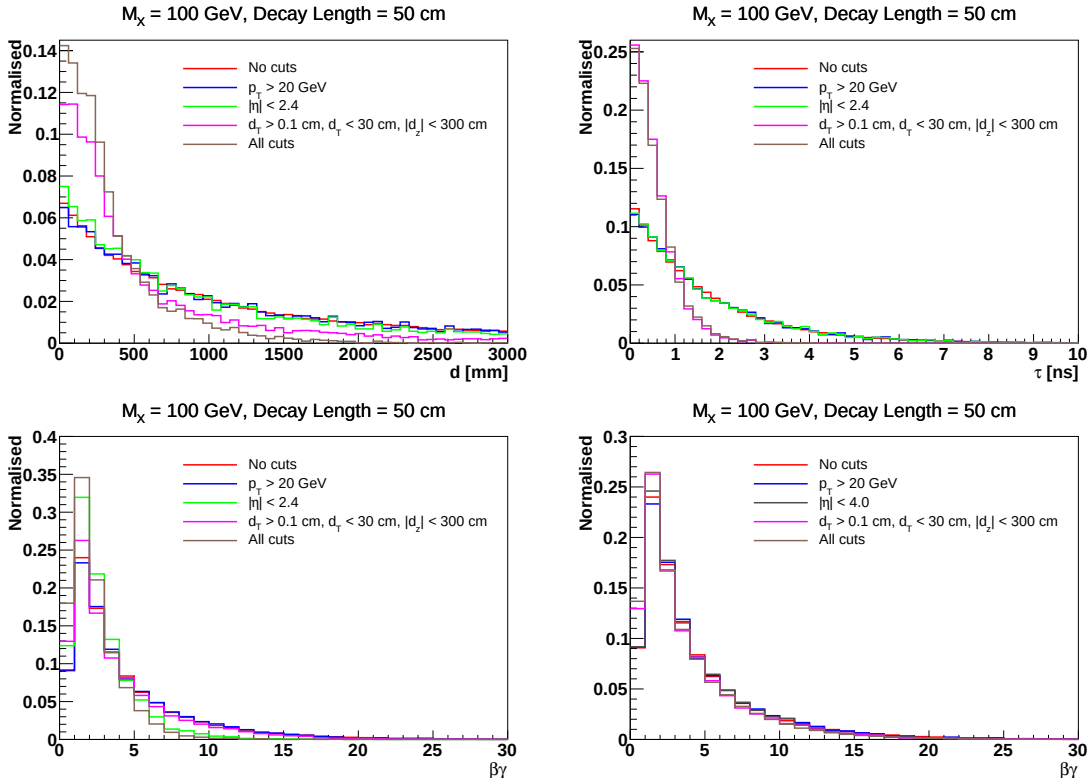

Figure 3: Effect of the cuts on the distribution of the reconstructed decay length d (upper left), the proper lifetime τ (upper right), and the the boost factor $\beta\gamma$ (bottom left and right for two different pseudorapidity cuts $|\eta| < 2.4$ and $|\eta| < 4.0$ respectively). The distributions have been obtained assuming a mass of 100 GeV and a proper decay length of 50 cm. In each panel, we indicate the specific cuts that have been applied.

Based on the discussion presented in Section 2, we now attempt to estimate the lifetime of the particle X through a simple exponential fit using the `TF1` class integrated in the `ROOT` environment [55]. The performance of this estimation depends both on the mean proper lifetime of the LLP and on its mass. To illustrate this dependence, we perform our fit assuming two different LLP masses, 100 GeV and 1 TeV, and three different mean decay lengths, 10 cm, 50 cm, and 1 m. The results of this exercise are summarised in Table 1, which shows the estimated lifetimes based on the samples without any cuts and with the various cuts applied for all six cases. For completeness, we also quote the number of events remaining after each set of cuts is applied, starting with a sample of 10 000 events [4].

[4]Throughout the remainder of this paper we will be starting with an initial number of 10,000 LLPs prior to the imposition of any cuts. For comparison, the cross-section for the Drell-Yan production of a pair of 300 GeV electrically charged $SU(2)$-singlet vector-like leptons (*cf e.g.* [23]) at the 14 TeV LHC is $\sim$ 20 fb, implying that at the HL-LHC we expect $\sim 120,000$ LLPs before applying any kinematic cuts.

M_X [GeV]	DL [cm]	Reconstructed DL		
		without cuts	with BC	with EC
100	10	9.95 ± 0.10	9.91 ± 0.13 [6117]	7.90 ± 0.10 [5385]
100	50	49.74 ± 0.51	49.55 ± 0.64 [6117]	15.88 ± 0.30 [2626]
100	100	99.48 ± 1.01	98.82 ± 1.29 [6117]	19.03 ± 0.48 [1570]
1000	10	9.97 ± 0.10	10.02 ± 0.10 [9546]	8.89 ± 0.08 [9052]
1000	50	49.88 ± 0.49	50.09 ± 0.51 [9546]	19.73 ± 0.26 [5234]
1000	100	99.85 ± 0.99	100.15 ± 1.02 [9546]	22.62 ± 0.35 [3242]

Table 1: Lifetime estimates obtained from exponential fitting of the τ distribution for six combinations of LLP mass (M_X, in GeV) and decay length (DL, in cm) based on an initial sample (without cuts) of 10000 events. We indicate the reconstructed decay lengths $d = c\tau$ (in cm) together with the number of events (in brackets) remaining after each set of cuts (BC or EC) is applied.

We observe that although the LLP mean decay length can be accurately reconstructed when the BC sample is used, once the (necessary) Extra Cuts are applied the result of the fitting procedure becomes incompatible with the actual underlying value. The situation becomes worse when the true decay length is large, since a larger fraction of the decays occurs beyond the limit of $d_T < 30\,\text{cm}$. The induced bias leads to results which can deviate from the actual decay length by almost one order of magnitude. The situation becomes marginally better when the mass of the LLP increases, since heavier LLPs are characterised by smaller $\beta\gamma$ values, but it is clear that a naive exponential fit to the data does not constitute a viable option to reconstruct the LLP lifetime.

One idea in order to remedy this situation could be to try and reduce the EC-induced bias by restoring, as much as possible, the form of the distribution prior to their imposition. To this end, following the prescription described in Ref. [45], we can gradually restrict $\beta\gamma$ to smaller and smaller values. The rationale of this restriction lies with the fact that as the considered $\beta\gamma$ interval becomes narrower, the proportion of events characterised by large values of τ_i in the spectrum increases. If, below a certain value of $\beta\gamma$, the estimate of the decay length saturates, then we have identified the correct region, provided we have sufficient statistics (in practice, we never let the total number of events fall below 20). If the estimate does not saturate, then it is to be seen as a lower bound on the LLP decay length. In Figure 4, we show the result of this technique for the six benchmark configurations presented in Table 1.

We can see that this method does manage to provide a ballpark estimate for proper decay lengths of the order of 10 cm. Indeed, in this case the saturation of the reconstructed decay length is visible, the resulting interval does contain the true

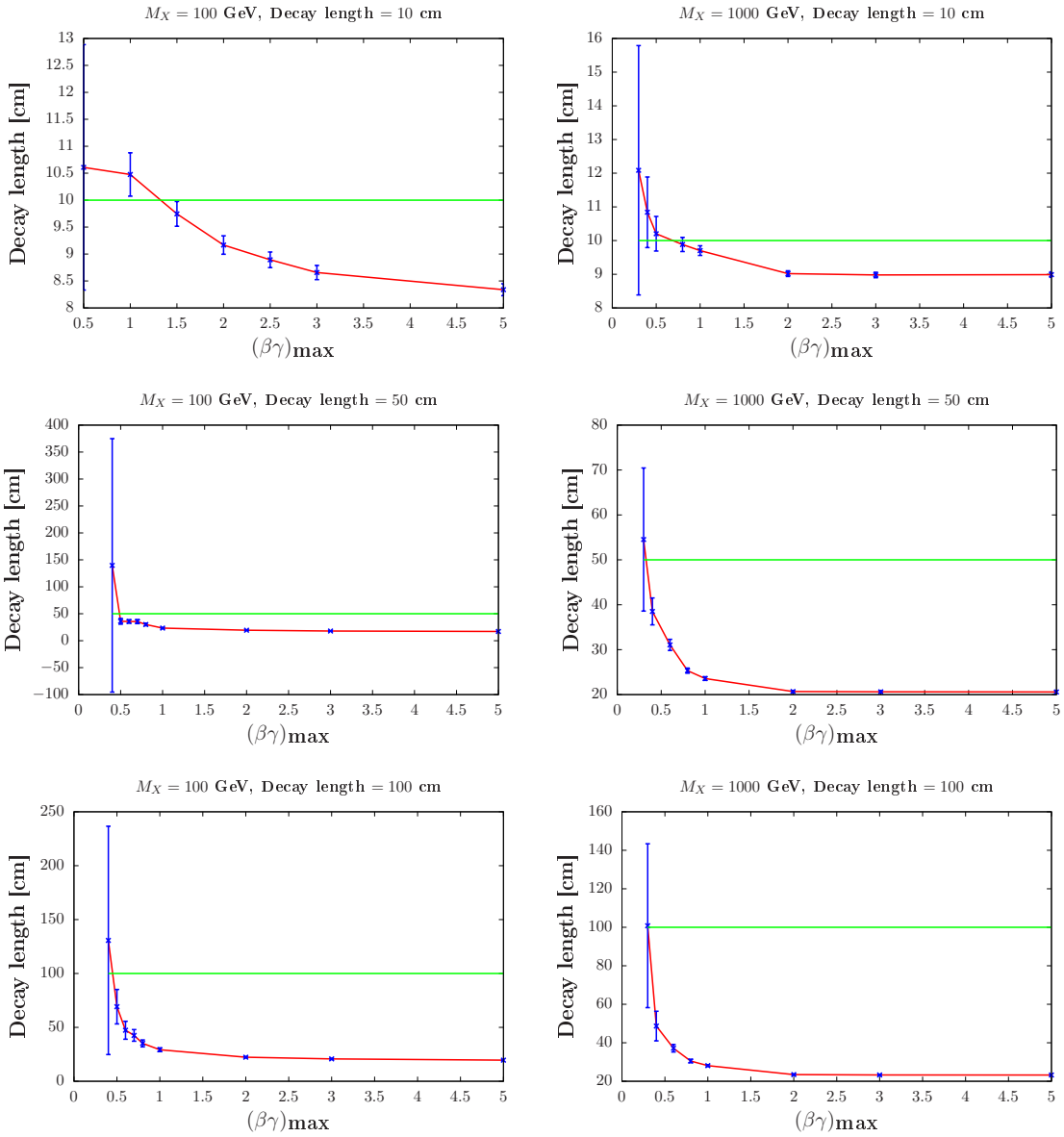

Figure 4: Reconstructed LLP decay length and with its associated uncertainty as a function of the restriction on $\beta\gamma$, for an LLP mass of $m_X = 100$ GeV (left) and $m_X = 1000$ GeV (right), and true decay lengths of 10 cm (top), 50 cm (middle) and and 100 cm (bottom).

value and the method yields a reasonable precision of the order of 30% or better. However, as the true value increases the method fails. Given that, moreover, it is difficult to make rigorous statistical sense out of this procedure, we believe that this method may be used in order to obtain a rough idea about the true proper lifetime of the LLP but cannot be used in the context of an actual experimental analysis.

3.1.2 Towards more realistic assessments

From the previous discussion we see that it is not possible to reconstruct the LLP lifetime in a fully model-independent manner based only on the measurement of its decay position, its mass, and its boost. The extra cuts (EC) introduce a bias towards smaller lifetimes in the sample because they restrict it to decays within a transverse distance of 30 cm from the beam line and hence reject decays characterised by larger proper lifetimes. Two approaches can be envisaged in order to circumvent this problem, which we will further develop in the subsequent sections. Note that, since the EC are imposed on the transverse decay length d_T, for convenience in everything that follows we will work exclusively with quantities defined in the transverse plane, namely d_T and the transverse boost factor $\beta_T\gamma$, both defined in Section 2.

The first approach requires minimal experimental information but incorporates theoretical bias, as it relies on a model-dependent χ^2 fitting. If, from experiment, we have the distribution of the transverse decay length d_T and the mass M_X of the LLP X, then we can simulate the process for that particular mass within the framework of a concrete model. Simulating events for different lifetimes and performing a binned χ^2 analysis of the d_T distribution, we can obtain an estimate for the actual lifetime of X. The results that can be obtained in this way will be presented in Section 3.1.3.

The second approach is also based on a χ^2 analysis. In contrast to the previous method it is fairly model-independent, but requires additional experimental information. To be more precise, along with the d_T distribution, we will assume that we can obtain the transverse boost factor ($\beta_T\gamma$) distribution of X from experiment. It is then possible to fit the (normalised) $\beta_T\gamma$ distribution by an appropriate function and use the latter as a probability density function to generate random numbers. As a second step, random numbers will also be generated for each $c\tau$ distribution. Then, multiplying the two sets of random numbers leads to the d_T distribution for that particular lifetime. Based on this, we can vary the lifetime and perform a χ^2 analysis comparing the experimental d_T distribution and the one generated using the procedure we just described to estimate the actual lifetime of X. This method will be discussed in Section 3.1.4.

3.1.3 χ^2 fitting of $\beta_T\gamma c\tau$ distribution: model-dependent analysis

Let us start with the model-dependent approach. For the case where LLP decays into lepton pairs, the transverse decay length distribution and the LLP mass M_X can be experimentally measured. Then, within the framework of a concrete model, we can simulate the process assuming different lifetimes and perform a χ^2 analysis in a straightforward manner. The minimum of the resulting χ^2 distribution provides an estimate for the lifetime of the LLP. The reason why some knowledge about the underlying model is useful is because, as already mentioned above, the $\beta\gamma$ distribution

depends on the production mechanism and the decay length distribution is generated at the Monte-Carlo level by multiplication of the former with the lifetime distribution.

From now on we restrict our analysis to four out of the six benchmarks given in Table 1, which are characterised by mean proper decay lengths of 10 cm or 50 cm. For each configuration, we generate 10 000 events and apply the EC on the obtained samples. The events passing these cuts constitute the "experimental" d_T distributions that we wish to fit. To this end, we generate the same process with the LLP mass set equal to the invariant mass of the two final state electrons and varying the lifetime. For each lifetime, we generate 100 000 events and then apply the EC. We construct a d_T distribution with the same bin size as the distribution coming from the experiment. Here, we have set the bin size to 1 cm. We then calculate the χ^2 value between these two distributions as

$$\chi^2 \;=\; \sum_{i=1}^{N} \frac{(n_{\rm th} - n_{\rm exp})^2}{\sigma^2} \;=\; \sum_{i=1}^{N} \frac{(n_{\rm th} - n_{\rm exp})^2}{(b-a)^2}\,, \tag{3.1}$$

where N is the total number of bins in the distribution, and $n_{\rm exp}$ and $n_{\rm th}$ are the experimentally observed and theoretically expected number of events in each bin. The expected number of events in each bin ($n_{\rm th}$) is normalized to the total number of events observed in experiment. The denominator is the square of the 68% confidence level uncertainty in the observed number ($n_{\rm exp}$), which is equal to the difference between the 68% upper (b) and lower (a) limits on the value of $n_{\rm exp}$. The latter are given by

$$\begin{aligned} a &= \frac{1}{2} F^{-1}_{\chi^2}\Big[0.32,\, n_d = 2n_{\rm exp}\Big]\,, \\ b &= \frac{1}{2} F^{-1}_{\chi^2}\Big[0.68,\, n_d = 2\big(n_{\rm exp}+1\big)\Big]\,, \end{aligned} \tag{3.2}$$

where $F^{-1}_{\chi^2}$ is the quantile of the χ^2 distribution with the number of degrees of freedom for the χ^2 distribution given by n_d [56].

In our simulation, we vary the mean proper decay length between 1 cm and 150 cm with a step size of 1 cm. Figure 5 shows the resulting χ^2 distributions as a function of the decay length for the four cases. The reconstructed lifetimes, corresponding to the χ^2 minimum are summarized in Table 2 together with the 1σ and 2σ lower and upper limits on the lifetime in each case. Here, the number of degrees of freedom (dof) for the χ^2 analysis has been taken to be one less than the number of bins over which the sum in Eq. (3.1) has been carried out ($N = 30$, $dof = 29$).

We observe that the mean proper lifetime can be reconstructed with a precision of about 10% for decays lengths of the order of 10 cm, whereas for 50 cm we obtain the lifetime within roughly a factor of 2. Note also that, again, with increasing mass the χ^2 minimum becomes more prominent.

The results shown in Table 2 have been obtained using the same model as the one that was used in order to generate our pseudo-experimental sample. A reasonable

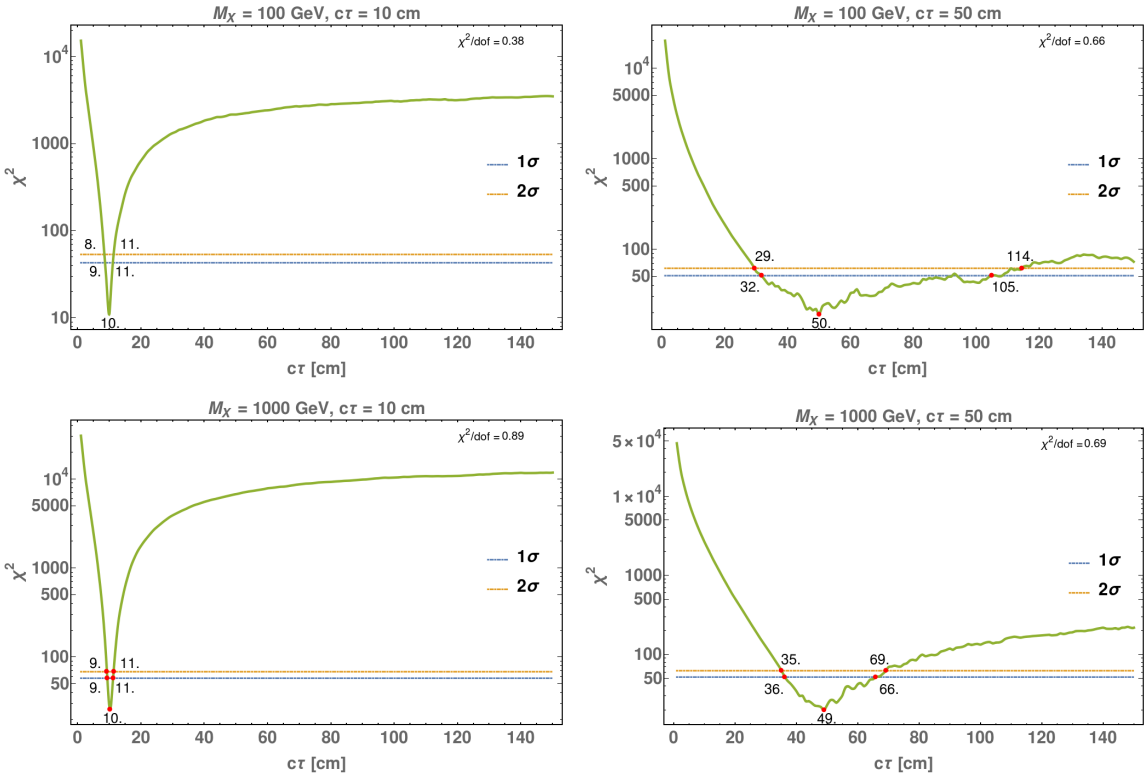

Figure 5: Model-dependent χ^2 as a function of the reconstructed decay length $c\tau$ for LLP masses of 100 GeV (top) and 1000 GeV (bottom) and decay lengths of 10 cm (left) and 50 cm (right). The χ^2 is based on the data samples after applying the EC for the displaced lepton signature.

M_X (GeV)	DL (cm)	Rec. DL (cm)	1σ LL (cm)	1σ UL (cm)	2σ LL (cm)	2σ UL (cm)
100	10	10	9	11	8	11
100	50	50	32	105	29	114
1000	10	10	9	11	9	11
1000	50	49	36	66	35	69

Table 2: Lifetime estimates by model-dependent χ^2 fitting of the d_T distribution (as shown in Figure 5) for the displaced leptons signature assuming different combinations of the LLP mass M_X and decay length (DL). We display the reconstructed decay length as well as the corresponding lower (LL) and upper (UL) limits at the 1σ and 2σ confidence level, respectively.

question would be to ask how would these results change if we assumed the wrong model, like a different production mode of the LLP X. In this case, we will obtain the wrong lifetime estimate but with comparable error bands. For example, if the actual underlying process was production of X from the decay of an on-shell resonance, and

we had assumed non-resonant production, then the χ^2 analysis would give minima at a wrong decay length due to difference in the boost factor distributions of the two processes. However, it is possible to identify such resonant LLP production and the mass of the intermediate resonance, if any, from the total invariant mass distribution of the two LLPs' decay products. Moreover, the spin information of LLP X can also be inferred from the angular distributions of its decay products as discussed in Ref. [57] for slepton and in Refs. [57–59] for the Higgs boson. Hence, it is possible to deduce several key features of the underlying model if we can reconstruct all the decay products of the LLP pair. Even for decays of LLPs involving invisible particles, there are methods to identify the model and its parameters, like the LLP mass, as we will discuss later.

3.1.4 χ^2 fitting of $\beta_T\gamma c\tau$ distribution: model-independent analysis

Let us now turn to our model-independent method which, however, requires certain additional experimental information. As we already mentioned in Section 3.1.2, here we will assume that the $\beta_T\gamma$ and d_T distribution can be extracted from experiment. This distribution will be fitted with a suitable function which, if treated as a probability density function, can be used to generate a large number of random values for $\beta_T\gamma$. In Figure 6 we show the normalised $\beta_T\gamma$ distribution we obtain for benchmark $(m_X, c\tau) = (100\text{ GeV}, 10\text{ cm})$, along with the corresponding fit. Moreover, we employ an additional function of the form $-c\tau \ln U[r]$, where $U[r]$ generates a random number distributed uniformly between 0 and 1, to generate exponential lifetime distributions with different values for $c\tau$. Multiplying the two sets of random numbers, we obtain a d_T distribution for various combinations of $\beta_T\gamma$ and $c\tau$. This d_T distribution can then be used to perform a χ^2 analysis similar to the one described in Section 3.1.3 and obtain an estimate of the LLP lifetime. In this case, no specific model assumption is needed, since the knowledge of the $\beta_T\gamma$ distribution encapsulates all the necessary model information. Therefore, this is indeed a model-independent approach, provided that the information on $\beta_T\gamma$ is experimentally accessible.

Figure 7 shows the χ^2 distribution obtained through this method as a function of the reconstructed decay length for the same four benchmark configurations as in Section 3.1.3. Table 3 shows the reconstructed decay length and the 1σ and 2σ lower and upper limits for each scenario. Similar to the model-dependent χ^2 analysis presented previously, the number of degrees of freedom has been taken to be $dof = N - 1 = 29$.

Our findings show that for LLPs characterized by relatively short lifetimes or heavy LLPs, through this method it is possible to reconstruct the mean decay length with a comparable precision as when knowledge of the underlying model is assumed. For longer lifetimes and lower masses, and within the lifetime interval that we considered, we could only infer a lower limit from this χ^2 analysis as can seen in the upper right panel of Figure 7. Again with increasing mass, the lifetime estimation

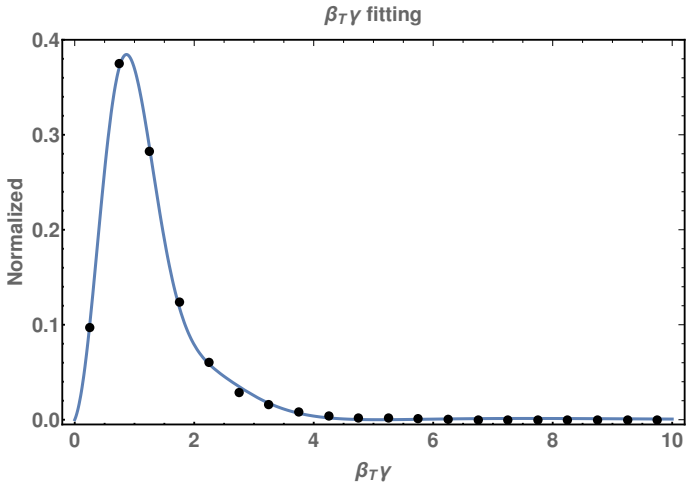

Figure 6: Fit of the normalized $\beta_T\gamma$ distribution for the benchmark $(m_X, c\tau) = (100\text{ GeV}, 10\text{ cm})$ using a function of the form: $A\,e^{-x}x - B\,e^{-x^2}x - C\,e^{-x}x^2 + D\,e^{-x^2}x^2 - E\,e^{-x^2}x^3 + F\,e^{-x}x^4$

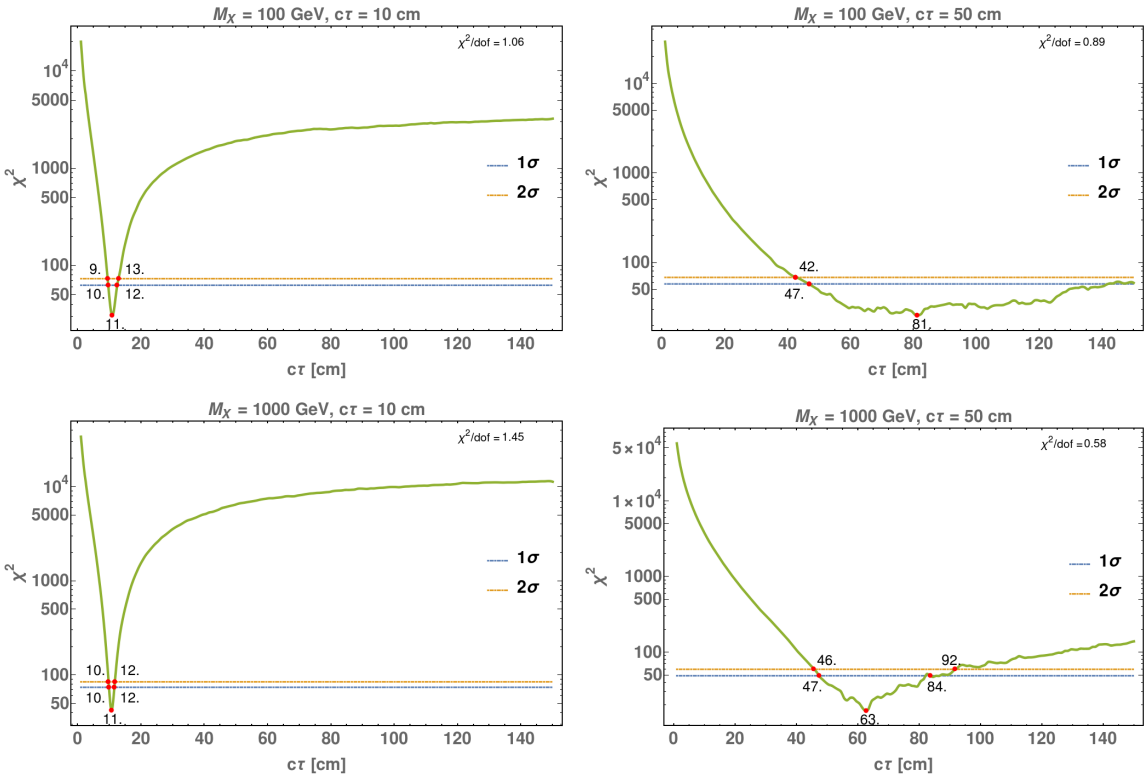

Figure 7: Model-independent χ^2 as a function of the reconstructed decay length $c\tau$ for LLP masses of 100 GeV (top) and 1000 GeV (bottom) and decay lengths of 10 cm (left) and 50 cm (right).

improves. These results are to be expected: as the mean proper lifetime and/or boost of the LLPs increases, the number of decays occurring within a radial distance

M_X (GeV)	DL (cm)	Rec. DL (cm)	1σ LL (cm)	1σ UL (cm)	2σ LL (cm)	2σ UL (cm)
100	10	11	10	12	9	13
100	50	81	47	> 150	42	> 150
1000	10	11	10	12	10	12
1000	50	63	47	84	46	92
$\eta < 4.0$ cut						
100	50	64	41	110	38	117

Table 3: Lifetime estimates by model independent χ^2 fitting of d_T distribution for displaced leptons signature.

of 30 cm from the beam line decreases. This means that our sampling of the $\beta_T\gamma$ distribution carries larger uncertainties which, in turn, reflect upon our capacity to reconstruct the LLP lifetime. In a sense, a model-dependent fit corresponds to the limit at which the $\beta_T\gamma$ distribution is known with infinite precision. Note also that the estimated lifetime using this method tends to be on the higher side because the $\beta_T\gamma$ distribution is affected by the cuts, as shown in fig. 3, and is biased towards lower values. Consequently, larger $c\tau$ values are favoured in order to match the experimental d_T distribution.

If we modify, along the guidelines envisaged for the High-Luminosity LHC, the cut on the pseudorapidity η such that $|\eta| < 4.0$, the results improve slightly for the case where the LLP mas is 100 GeV, as can be seen in Figure 8, where we repeat the same analysis with the modified cut on $|\eta|$. The reason is that, in a similar manner as previously, the $\beta_T\gamma$ distribution is affected less than if we adopt a tighter cut of $|\eta| < 2.4$ (*cf* the bottom-left and bottom-right panels of Figure 3). Therefore, with this extra pseudorapidity coverage, the $\beta_T\gamma$ distribution is less skewed and, hence, yields better estimations.

As mentioned in the introductory discussion, until now we have neglected all initial and final state radiation (ISR, FSR), multi-parton interactions (MPI), as well as smearing effects. In this Section we will repeat the model-independent χ^2 analysis in order to check the robustness of our results against these effects.

We therefore now consider processes where all of these effects are present. We do this by switching ISR, FSR and MPI effects on in `PYTHIA6` and then generate our sample. We also add a 10% smearing on the lepton transverse momentum. These effects affect the event sample in different ways. Initial state radiation can change the boost factor distribution of the long-lived particle, but this modified $\beta\gamma$ distribution can be reconstructed from the decay products of the LLP in a similar manner as when ISR is absent. The same is not true for final state radiation as this alters the momenta of the final decay products (in this case, the leptons) that we observe towards lower

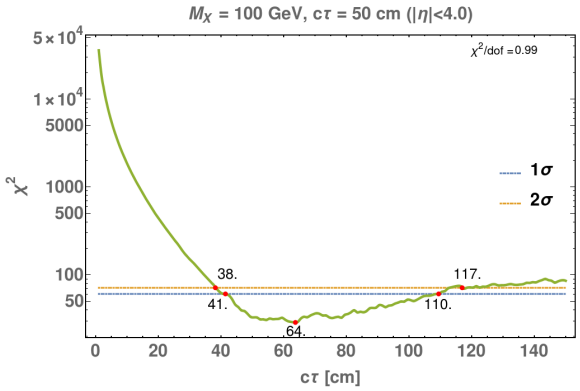

Figure 8: Model-independent χ^2 for an LLP mass of 100 GeV and a decay length of 50 cm as a function of the reconstructed decay length $c\tau$ assuming a pseudorapidity cut of $|\eta| < 4.0$ as envisaged for the High-Luminosity LHC.

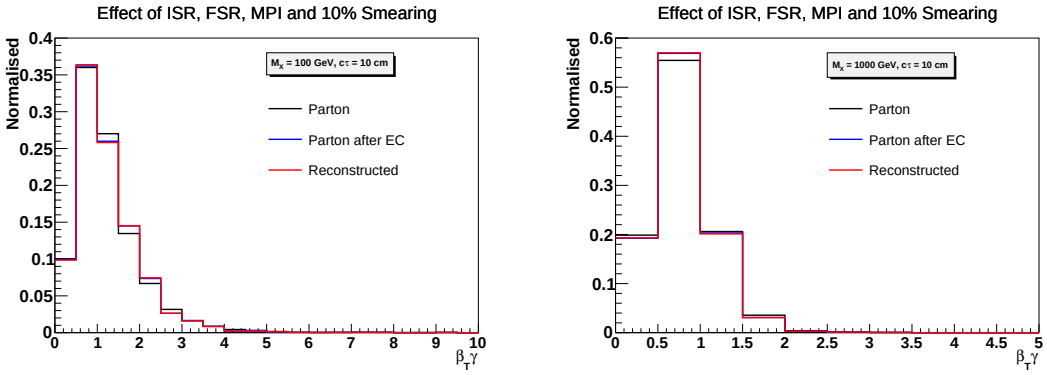

Figure 9: Effect of initial state radiation, final state radiation, multi-parton interaction and 10% smearing on the reconstruction of the $\beta_T\gamma$ distribution of an LLP of mass 100 GeV and 1000 GeV having decay length of 10 cm.

values and, hence, introduces a bias in the $\beta\gamma$ distribution. Multi-parton interactions, on the other hand, play no significant role here in changing the boost factor of the LLPs or their decay products. Finally, a smearing of the final lepton p_T will affect the reconstruction of the $\beta\gamma$ distribution of the LLP, but this effect does not lead to any particular trend towards lower or higher $\beta\gamma$ values. In Figure 9 we show the $\beta_T\gamma$ distribution of the LLP at the parton level before and after applying the EC set of cuts as well as the $\beta_T\gamma$ distribution of the LLP as reconstructed from its decay products after switching on ISR/FSR/MPIs and smearing, for an LLP of mass 100 GeV and decay length of 10 cm.

Our results for lifetime estimation are shown in Table 4. We observe that the reconstructed intervals are fairly consistent with our previous findings, implying that the analysis is robust against ISR, FSR, MPI and smearing effects.

M_X (GeV)	DL (cm)	Rec. DL (cm)	1σ LL (cm)	1σ UL (cm)	2σ LL (cm)	2σ UL (cm)
100	10	11	9	14	9	14
100	50	101	41	> 150	37	> 150
1000	10	10	9	12	8	12
1000	50	68	38	143	36	> 150

Table 4: Lifetime estimates by model-independent χ^2 fitting of d_T distribution for displaced leptons with ISR, FSR, MPI all switched on and a 10% smearing applied on the lepton p_T.

3.2 Displaced jets

Let us now move to the case of a neutral long-lived particle that decays into two quarks inside the tracker part of the detector. The observed LHC signature in this case consists of displaced jets. Since jets contain numerous charged particles, by extrapolating their tracks, it is possible to obtain the position of the secondary vertex quite accurately [51, 52]. In our analysis, we will assume that the positions of the secondary vertices are known with high precision and we will study the reconstruction of the mother particle's, *i.e.* the LLP's, $\beta\gamma$ from its decay products.

As in the displaced lepton case, we use `Pythia6` to generate events for pair-production of a long-lived particle X and its eventual decay into quarks. We discuss the reconstruction of the boost of the LLP from displaced jets and show that the situation becomes less straightforward than in the case of displaced leptons due to several complications affecting jet reconstruction. First, the mismatch between the actual energy of the quarks and the one measured from the jet affects the reconstruction of the $\beta_T\gamma$ distribution of the LLP. Secondly, the reconstruction of jets as their displacement increases may introduce additional challenges at the LHC. Concerning the second issue, since we are restricting ourselves to decays occurring within 30 cm from the beamline, we don't expect much difficulty in reconstructing the displaced jets. However, the measured jet energy can be quite different than that of the initial quark coming from the LLP decay. This may, in particular, affect the model-independent analysis which crucially depends on the fitting of the transverse boost distribution of the LLP.

3.2.1 Reconstructing $\beta_T\gamma$ of the LLP from displaced jets

We cluster energy depositions with $p_T > 5$ GeV and within pseudorapidity $|\eta| < 4.9$ (taking into account both the barrel and the endcap regions) of charged particles which do not come from the primary vertex as well as all neutral particles[5] to build

[5]Charged particles coming from the primary vertex can be identified in the tracker and can, hence, be removed. Neutral particles coming from the primary vertex cannot be identified and

jets with a minimum transverse momentum of 20 GeV and $|\eta| < 4.0$ (the HL-LHC pseudorapidity coverage of the tracker) using a cone of $R = 0.4$ [6]. We then identify charged particles coming from each secondary vertex and count how many of these particles are present in each jet. If a jet contains at least two particles from one secondary vertex and none from the other one, then that jet is associated with the former secondary vertex. If the number of jets associated with a particular secondary vertex is greater than two and if the invariant mass of all these jets falls within 40% of the mass of the mother particle, which can be inferred from the peak of the invariant mass distribution, then we use all such jets to reconstruct the $\beta_T\gamma$ of the corresponding mother particle. Here, we keep ISR, FSR and MPI all switched on and a 50% smearing on E_T is applied. In Fig. 10 we show the $\beta_T\gamma$ distribution of the LLP at the parton level before and after applying the EC, along with the one reconstructed from the displaced jets. We can see that the shape of the reconstructed distribution is, indeed, modified, which we expect to affect the model-independent lifetime estimation. This effect is expected for jets due to many effects like out-of cone radiation, energy smearing and energy resolution of the detector. In experiments, one usually applies jet energy correction factors to recover from these effects and get some matching between MC jets and detector jets, and this correction factor is a function of p_T and η. However, for displaced jets, this correction factor will be a function of displacement in addition to the p_T and η of these jets. Moreover, the patterns of energy deposition for displaced and prompt jets also have some differences and again depend on displacement, as has been studied in Ref. [60, 61]. Once this is calibrated, and applied to the jets, we can expect to get closer to the correct $\beta_T\gamma$ distribution. In this work, we present our analysis without applying any jet energy correction.

We now move on to the LLP lifetime reconstruction, first within a model-dependent and afterwards within a model-independent framework.

3.2.2 Reconstructing the lifetime: model-dependent χ^2 analysis

Let us first assume that the underlying model is known[7]. Note also that the mass of the LLP can be reconstructed from the dijet invariant mass. Once we assume the model, we only need to know the position of the SV in order to perform a χ^2 analysis as before. In the case of displaced jets, the SV can be identified more precisely than in the case of displaced leptons thanks to the greater number of charged particles involved in the process.

Our results are presented in Table 5, where we show the reconstructed decay lengths along with their 1σ and 2σ uncertainties for the same two LLP masses and

hence can contribute to a jet's energy.

[6] $R = \sqrt{\eta^2 + \phi^2}$

[7] Relevant information can be inferred, for instance, by observing various distributions of the final state jets.

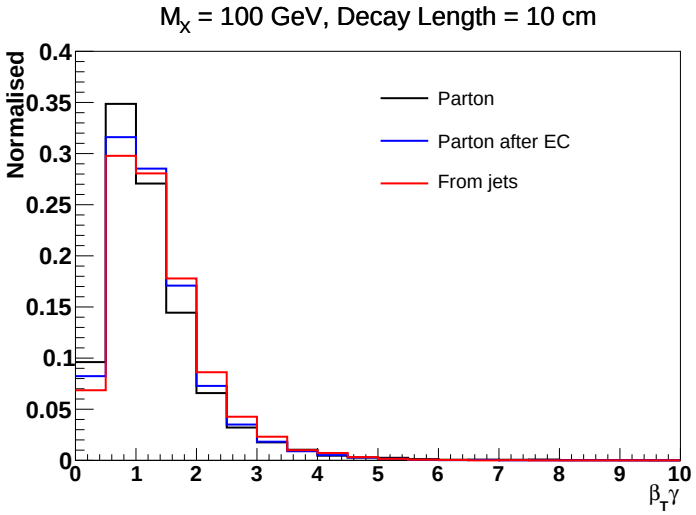

Figure 10: $\beta_T\gamma$ distribution of the LLP at the parton level before applying EC, after EC and that reconstructed from jets.

M_X (GeV)	DL (cm)	Rec. DL (cm)	1σ LL (cm)	1σ UL (cm)	2σ LL (cm)	2σ UL (cm)
100	10	10	8	12	8	12
100	50	53	30	> 150	28	> 150
1000	10	10	9	11	9	11
1000	50	58	39	83	38	95

Table 5: Lifetime estimates through a model-dependent χ^2 fit of the d_T distribution for displaced jets.

decay lengths as in the displaced lepton case. We find that for a LLP of mass 100 GeV and a decay length of 50 cm, through this type of analysis we can only infer a lower limit on the parent particle's proper decay length within the lifetime interval that we consider. For shorter decay lengths and/or heavier LLPs, however, the lifetime can be bounded both from above and from below with a precision of roughly $10\% - 20\%$ at 1σ.

3.2.3 Reconstructing the lifetime: model-independent χ^2 analysis

If the underlying model is unknown, much like in the displaced lepton case we need to assume that the $\beta_T\gamma$ distribution of the LLP can be measured experimentally. However, as we saw in Section 3.2.1, the $\beta_T\gamma$ distribution obtained from the final state displaced jets tends to deviate from the actual one. This will affect the lifetime estimation. In Table 6 we present the accuracy with which the LLP lifetime can be estimated in this framework.

We find that the lifetime reconstruction is poor when we use the naive $\beta_T\gamma$

M_X (GeV)	DL (cm)	Rec. DL (cm)	1σ LL (cm)	1σ UL (cm)	2σ LL (cm)	2σ UL (cm)
100	10	13	11	15	11	15
100	50	67	41	> 150	39	> 150
1000	10	14	13	15	12	15
1000	50	94	70	> 150	67	> 150

Table 6: Lifetime estimates through a model-independent χ^2 fit of the d_T distribution for displaced jets.

distribution from experiment, since the 2σ interval does not contain the actual decay length values, most of the time. A first way through which this situation could be improved would be by applying proper correction factors on the jets calibrated as a function of p_T, η and d_T of the jets as has been discussed in Section 3.2.1. An alternative idea could be to rely on timing information which will be available in the HL-LHC upgrade. The second option will be further discussed in Section 4.2.

3.3 Displaced leptons with missing transverse energy

We now consider the 3-body decay of a neutral long-lived particle (LLP) X into two leptons along with an invisible particle Y,

$$X \;\rightarrow\; \ell^+\ell^- Y.$$

The presence of more than one lepton implies that the position of the secondary vertex (SV) can be identified. But in this class of LLP decays, measuring the $\beta\gamma$ of X is more challenging since not all the decay products can be reconstructed. Hence, we need a lifetime estimation method which does not rely on the knowledge of the $\beta\gamma$ information of the LLP. To the best that we can think of, the only option in order to reconstruct the LLP lifetime in this class of decay modes is a model-dependent analysis.

An additional complication arises due to the lack of knowledge concerning the LLP mass. One possibility is to employ the dilepton invariant mass edge, which is determined by the difference between the mass of the LLP and that of the invisible particle

$$M_{\ell\ell}^{\text{edge}} \;=\; m_X - m_Y \;=\; \Delta \tag{3.3}$$

and to assume that particle Y is massless. We can then indeed estimate the mass of X from the edge of the dilepton invariant mass distribution. After determining the mass, we can follow the same procedure as in the case of displaced leptons.

The massless invisible particle assumption can be avoided by employing the stransverse mass (MT2) variable to find out the masses of the mother particle as

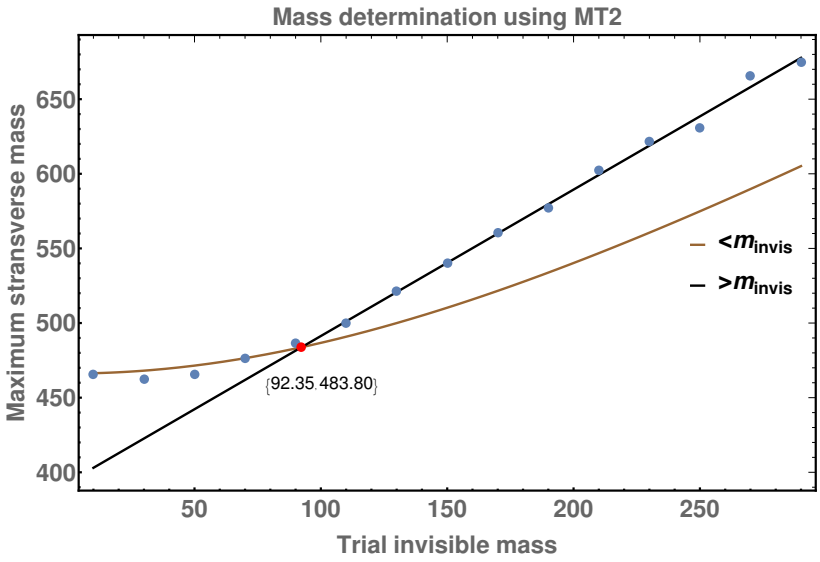

Figure 11: Mass determination of the LLP and the invisible particle using the stransverse mass variable for cases where the intermediate particle is off-shell.

well as its invisible decay product as has been shown for the case of gluino decaying to neutralino and jets in Ref. [62]. The transverse mass of a gluino is given as

$$m_T^2(m_{T,vis}, m_Y, \mathbf{p}_T^{vis}, \mathbf{p}_T^Y) = m_{T,vis}^2 + m_Y^2 + 2(E_T^{vis} E_T^Y - \mathbf{p}_T^{vis} \cdot \mathbf{p}_T^Y) \tag{3.4}$$

where $m_{T,vis}$ and $\mathbf{p}_T^{vis}$ are the transverse invariant mass and transverse momentum of the visible system, respectively, while m_Y and $\mathbf{p}_T^Y$ are the assumed mass and transverse momentum of the invisible system, respectively. Each event will involve two such LLP decays and the stransverse mass variable (MT2) is defined as

$$m_{T2}^2 \equiv \min_{\mathbf{p}_T^{Y(1)} + \mathbf{p}_T^{Y(2)} = \mathbf{p}_T^{miss}} \left\{ \max\left\{ m_T^{2(1)}, m_T^{2(2)} \right\} \right\}, \tag{3.5}$$

where the maximum transverse mass of the two LLPs in each event is minimised over all possible values of $\mathbf{p}_T^{Y(1)}$ and $\mathbf{p}_T^{Y(2)}$ such that they always satisfy $\mathbf{p}_T^{Y(1)} + \mathbf{p}_T^{Y(2)} = \mathbf{p}_T^{miss}$. The edge of the transverse mass distribution (i.e. m_{T2}^{max}) gives the value of the LLP mass only if the correct mass of the invisible particle is used in Equation (3.4). Otherwise, m_{T2}^{max} has a different functional dependence on m_Y depending on whether its value is smaller or greater than the actual invisible particle mass. The two functions, however, intersect at the invisible particle mass. As it has been shown in Ref. [62], this feature can be used in order to deduce the mass of the LLP. In Figure 11 we show the variation of the maximum stransverse mass with varying trial masses for the invisible particle fitted with two different functions and how the intersection of these functions can provide an estimate of both the LLP and invisible particle's masses.

M_X (GeV)	DL (cm)	Rec. DL (cm)	1σ LL (cm)	1σ UL (cm)	2σ LL (cm)	2σ UL (cm)
100	10	9	7	15	6	15
100	50	34	14	> 150	12	> 150
1000	10	10	9	11	9	11
1000	50	45	33	67	32	72

Table 7: Lifetime estimates by model-dependent χ^2 fitting of d_T distribution for displaced leptons plus $\not{E}_{\rm T}$ final state.

The reconstructed masses are 483.8 ± 4.57 GeV and 92.35 ± 8.62 GeV for a 500 GeV LLP decaying into a 100 GeV invisible particle. Note that here we have performed a very simplistic analysis without considering any detector effects just to illustrate that it is possible to get at least a ballpark estimate of the particle masses even for signatures including missing transverse energy (even in the absence of timing). With the LLP and invisible masses at hand, and within the framework of a specific model, we can then perform a model-dependent χ^2 analysis to reconstruct the LLP lifetime. It should be noted that the same method can also be applied to the case in which the LLP decays to two leptons and an invisible particle through an on-shell intermediate particle. For further details of this analysis the reader is referred to Ref. [62].

In Table 7 we present the reconstructed lifetime values along with their 1σ (68% CL) and 2σ (95% CL) lower and upper limits for the GMSB model presented in Section 3. We observe that the true lifetime can be reconstructed with a precision of 40% (at 68% CL) for small masses and lifetimes, improving to roughly 15% for heavier (*i.e.* less boosted) LLPs. For longer lifetimes the latter number translates to roughly 40%, whereas for a light LLP with a longer lifetime we could only infer a lower limit on $c\tau$ within the considered interval.

3.4 Charged LLP decaying to lepton and invisible particle

The last case we consider is that of a charged LLP decaying into a lepton and an invisible particle inside the tracker. If the mass difference between the charged LLP and the invisible particle is substantial, then the lepton will have sufficient transverse momentum and can be reconstructed, giving rise to a "kinked" track signature. If, on the other hand, the charged LLP and the invisible particle are degenerate in mass, the lepton will be too soft to be reconstructed, leading to a disappearing track in the Tracker. Here we will focus on the former case.

In the busy environment of the LHC, online triggering on a kinked track is challenging [63], especially if the LLP decay occurs towards the outer parts of the Tracker system. However, as stated in Ref. [63], off-line reconstruction of this kink

M_X (GeV)	DL (cm)	Rec. DL (cm)	1σ LL (cm)	1σ UL (cm)	2σ LL (cm)	2σ UL (cm)
100	10	8	7	10	7	10
100	50	67	33	121	30	133
1000	10	10	9	11	9	11
1000	50	50	35	71	33	78

Table 8: Lifetime reconstruction through a model-dependent χ^2 fit of the d_T distribution for kinked tracks.

could be attempted, which would then provide the position of the SV with some uncertainty. Moreover, from the track of the charged LLP we can calculate its momentum, while the rate of energy loss due to ionisation (*i.e.* the LLP's dE/dx) can be used to estimate its mass. Then, it is – at least in principle – possible to retrieve all the information that is necessary in order to reconstruct the lifetime in a similar manner as we did for displaced leptons, and we can use any of the alternatives to estimate the lifetime.

Note that until now we have not discussed issues related to the efficiency with which displaced objects can be detected. Given the exceptionally challenging nature of the kinked tracks, however, it is important to try and estimate, even in a crude manner, the efficiency of reconstructing such a signature in the first place. To this goal, in what follows we will assume that the probability to reconstruct a kinked track can be expressed as a convolution of three factors: first, the efficiency to identify the charged LLP track. This can be typically identified with about 95% efficiency if the LLP travels a distance of at least 12 cm before decaying, as shown in Ref. [64]. Secondly, the efficiency of identifying the (displaced) lepton track. We take this to be identical as for ordinary displaced leptons, and borrow it from Ref. [65]. Finally, in order to be able to disentangle the two tracks, we also demand that the angular separation (ΔR) between the LLP and the lepton should be greater than 0.1 radian, so that the kink is prominent.

3.4.1 Model-dependent χ^2 analysis

With the previous remarks in mind, we first perform a model-dependent χ^2 analysis. In Table 8 we show the reconstructed decay length values for our four benchmarks along with the 1σ and 2σ lower and upper limits on the LLP lifetime for each scenario.

We see that a lifetime $c\tau = 10$ cm can be reconstructed with a precision of $\sim 15\%$ (65% CL) for a 100 GeV LLP, which turns to 10% for a 1 TeV particle. As expected, the precision decreases as $c\tau$ increases but, for $c\tau = 50$ cm we can still obtain results within a rough factor of 2.

M_X (GeV)	DL (cm)	Rec. DL (cm)	1σ LL (cm)	1σ UL (cm)	2σ LL (cm)	2σ UL (cm)
100	10	11	9	12	9	13
100	50	71	45	> 150	41	> 150
1000	10	10	9	11	9	11
1000	50	59	47	93	43	101

Table 9: Lifetime reconstruction through a model-independent χ^2 fit of the d_T distribution for kinked tracks.

3.4.2 Model independent χ^2 analysis

Let us now move to our model-independent analysis. One important point to note here is that the transverse decay length distribution as obtained from experiment is expected to be biased towards lower values because of the dependence of the displaced lepton track reconstruction efficiency on the decay length - the efficiency decreases as d_T increases. Since, however, these efficiencies *are* known, it should be possible to unfold the experimental d_T distribution accordingly and then compare with the distributions that we obtain using the product of various $c\tau$ distributions with the fitted $\beta\gamma$ distribution[8].

In Table 9 we present the reconstructed lifetime value for each of our benchmarks, along with their 1σ (68%) and 2σ (95%) lower and upper limits.

We observe that for all of our benchmarks, it is possible to obtain a reasonable reconstruction of the LLP lifetime, with a precision that is comparable to the one obtained through the model-dependent analysis presented in the previous Section.

4 Including timing information

The proposal for a MIP Timing Detector (MTD) [66] for the phase II CMS upgrade, which will provide the timing information for MIPs (minimum ionizing particles), can provide additional information which is relevant for the lifetime reconstruction of LLPs. A few recent works have already studied aspects of the role that such a detector could play in LLP searches [67, 68]. It has also been shown in Refs. [5, 69] that timing information can help in measuring the mass of the LLPs.

The proposed design for MTD indicates that it will be able to provide timing measurements for all charged particles having $p_T > 0.7$ GeV in the barrel region ($|\eta| < 1.5$) and $p > 0.7$ GeV in the endcaps (up to $\eta = 3$) with a time resolution of 30 ps. It will be placed at a radial distance of 1.161 m from the beam axis [66]: in the transition region from the tracker to the ECAL.

[8] A similar remark also applies to the displaced leptons and displaced jets analyses of the previous Sections.

In what follows we will use the `ParticlePropagator` functionality of the `Delphes 3.4.1` [70] package to get the timing of the charged particles coming from an LLP decay, restricting ourselves to the barrel region and applying a 30 ps Gaussian smearing on the time obtained from `ParticlePropagator`. Our goal is not to repeat the analyses performed in the previous Sections. Instead, we will simply comment on the role that the MTD could play in the LLP mass reconstruction and in the estimation of its lifetime in the various scenarios we examined previously.

4.1 Mass reconstruction

In Sec. 3.3, we saw that when the LLP decay involves an invisible particle, the LLP mass can be reconstructed by employing the stransverse mass variable. In the case of a three-body decay of the LLP into two visible particles along with an invisible one, we can also get the mass difference of the LLP and the invisible particle from the edge of the invariant mass distribution of the two visible decay products.

However, when the LLP decays into an invisible particle along with an *on-shell* intermediate neutral particle (which, in turn, decays visibly), the invariant mass of the visible part of the decay will peak at the intermediate particle's mass and, therefore, we cannot rely on the mass edge to obtain the difference between the LLP and the invisible particle's mass.

In this section, we discuss how the mass reconstruction could improve in these two cases once timing information from the MTD is taken into account.

4.1.1 Two-body decay of the LLP involving an invisible particle

Consider the following decay of an LLP X:

$$X \to Z\, Y\,, \;\; Z \to l^+ l^-$$

where Y is an invisible particle. Here the dilepton invariant mass will peak at the SM Z boson mass. However, using information from the MTD and the position of the SV, we can find out the boost of the LLP using the relation

$$\frac{l_1}{\beta_X} + \frac{l_2}{\beta_l} = ct \tag{4.1}$$

where l_1 is the distance travelled by the LLP from the PV to the SV where it decays and l_2 is the length traversed by the charged decay product (here, the lepton) from the SV to the point where it hits the MTD, β_X and β_l are the boosts of the LLP and the charged decay products respectively, t is the time when the charged particle hits the MTD, and c is the speed of light.

Once we know the LLP boost, we can boost back the leptons to the rest frame of the LLP. In this frame, the following relation holds

$$m_X^2 + m_{\rm vis}^2 - m_Y^2 = 2 m_X E_{\rm vis}^{\rm rest} \tag{4.2}$$

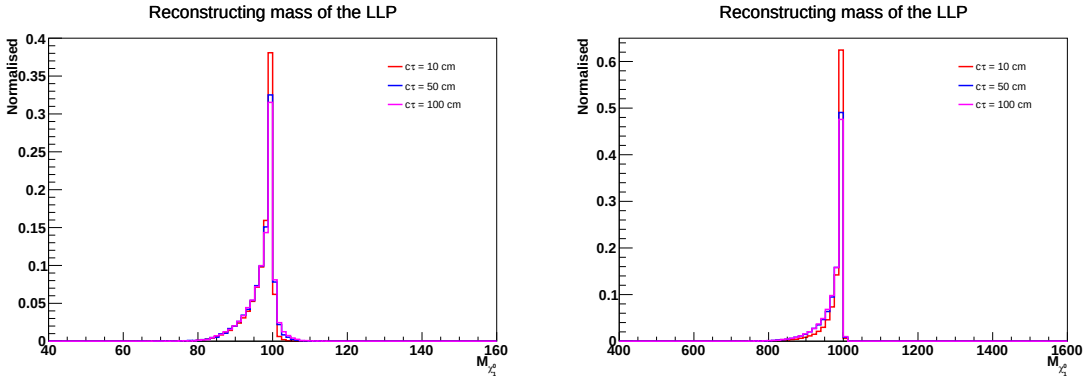

Figure 12: Reconstruction of the LLP mass for the decay of the LLP, neutralino, into Z and gravitino and further decay of Z into electrons for an LLP mass of 100 GeV (left) and 1000 GeV (right).

where m_{vis} and $E_{\text{vis}}^{\text{rest}}$ are the mass of the visible system (here, the dilepton invariant mass which peaks at Z mass) and the total energy of the visible decay products in the LLP rest frame. If, now, we assume that the invisible particle is (quasi-)massless, then the mass of the LLP can be estimated using

$$m_X = E_{\text{vis}}^{\text{rest}} + p \tag{4.3}$$

For concreteness, let us consider the decay of a neutralino (LLP) into a leptonically decaying SM Z boson and a gravitino (invisible). We consider two different masses of the neutralino – 100 GeV and 1000 GeV. In Figure 12 we show the reconstruction of the LLP mass assuming the gravitino to be massless and using Eq. (4.3).

The longer tail of the distribution towards lower masses is due to the mismatch between the azimuthal angle ϕ and pseudorapidity η of the decay products measured at the collider and the actual $\eta - \phi$ value (which starts from the SV) of the displaced electrons.

In order to circumvent the assumption that the invisible particle is massless, we can try to actually *reconstruct* the two masses (LLP/invisible particle) by observing that Eq. (4.2) holds on an event-by-event basis. Then, by solving it for different pairs of events, we can obtain an estimate of the two masses. We expect this method to work for cases where the intermediate particle has a non-vanishing decay width and, therefore, Eq. (4.2) will involve slightly different values of m_{vis} and $E_{\text{vis}}^{\text{rest}}$ for each event (otherwise we simply obtain the same equation each time). However, the addition of final state radiation and smearing will affect the solutions because these effects will bias the parameters of Eq. (4.2) in different ways in each event. In Fig. 13 we show the mass reconstruction of the LLP and the invisible particle by solving Eq. (4.2) for every two observed events with final state radiation switched on and a smearing of 5% on the leptons. We observe that the reconstruction is,

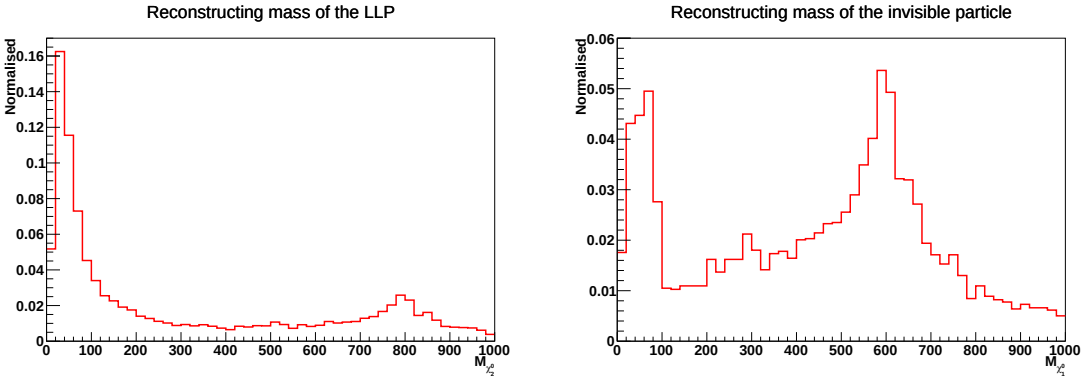

Figure 13: Reconstructing the LLP mass (left) and the invisible particle mass (right) by solving Eq. (4.2) for every two observed events where the actual LLP and invisible particle masses are 500 GeV and 100 GeV respectively.

indeed, affected but we deduce that the massless invisible particle assumption may be possible to drop. Note that the large number of solutions populating the low mass regions in both panels of Fig. 13 are a result of final state radiation which reduces the energy of the visible decay products.

4.1.2 Three-body decay of the LLP involving invisible particle

Let us now consider the three-body decay of an LLP X as:

$$X \to l^+ \, l^- \, Y \,, \tag{4.4}$$

where Y is an invisible particle. In Sec. 3.3 we discussed one method through which both the mass of the LLP and that of the invisible particle can be reconstructed. By employing timing information, an alternative approach can be envisaged. Namely, in this case, we have another equation (Eq. (4.2)) in the rest frame of the LLP, which can be solved along with Eq. (3.3) in order to obtain simple expressions for both masses as

$$m_X \;=\; \frac{\Delta^2 - M_{ll}^2}{2(\Delta - E_{\rm vis}^{\rm rest})} \,, \qquad\qquad m_Y \;=\; m_X - \Delta \,. \tag{4.5}$$

As an example, let us consider the three-body decay of a neutral LLP into two muons along with an invisible particle. The mass of the LLP has been set to 200 GeV and the invisible particle's mass is set to 50 GeV. The decay length of the LLP in this case is set to 10 cm.

In the top panel of Fig. 14, we show the dimuon invariant mass distribution. The edge of the distribution corresponds to Δ, which in this case is 150 GeV. Using this value of Δ and Eq. (4.5), we can indeed calculate both m_X and m_Y. In the lower panels of Fig. 14 we show the reconstructed mass of the LLP and that of the invisible system, respectively. Therefore, timing can help in mass reconstruction of

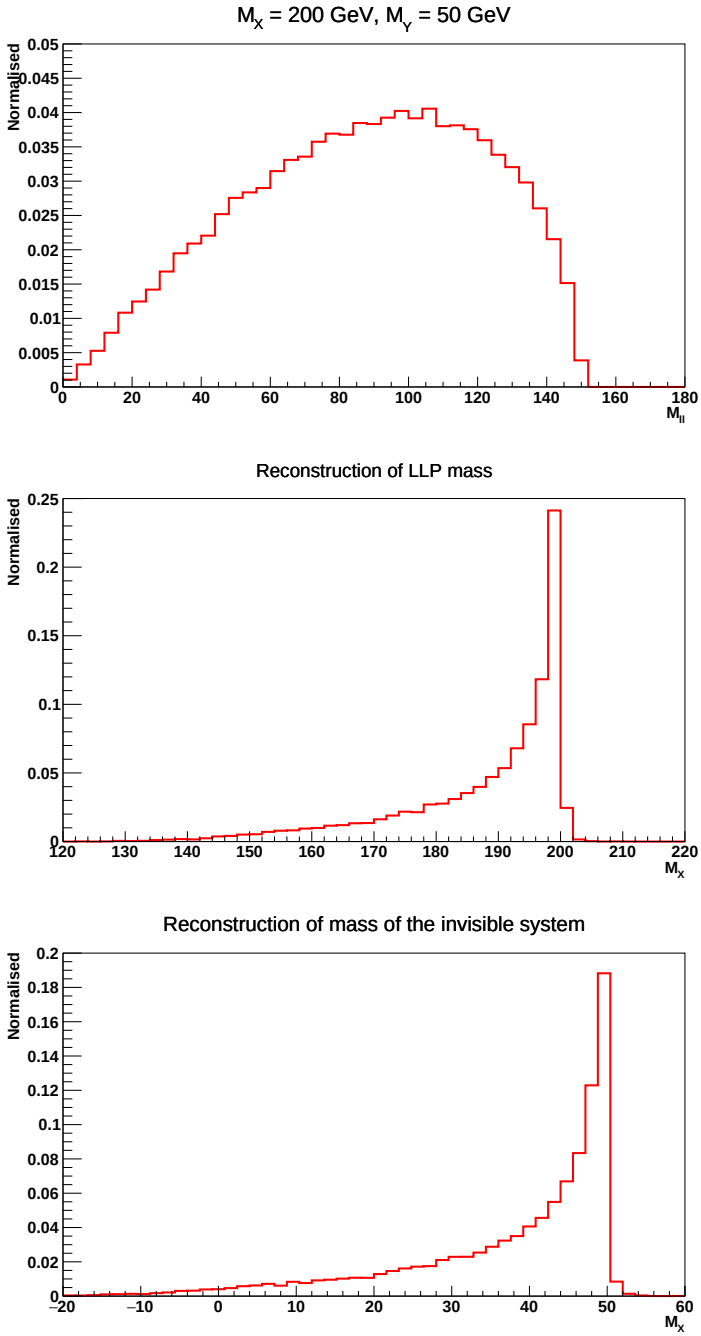

Figure 14: Estimation of the difference between LLP mass and the mass of the invisible system from dimuon invariant mass edge (top), reconstruction of the LLP mass (centre) and the invisible system's mass (bottom), respectively, using timing information.

LLPs as well as the invisible particle coming from the LLP decay, even if we do not use the missing transverse energy information [9].

[9]If we have timing information available at ILC as well, given that its potential to reconstruct

4.2 Improving the lifetime estimation

The inclusion of timing information for charged particles enables us to calculate the boost of the LLP if the position of the secondary vertex is known, even when we cannot reconstruct all of its decay products. This is particularly useful in order to estimate the LLP lifetime when the final state particles' energy and momentum are significantly smeared, as in the case of displaced jets, or when there are invisible particles in the final state. In this Section we will compare the parton-level transverse boost factor ($\beta_T\gamma$) distributions with the ones obtained using MTD timing information in these two cases.

4.2.1 LLPs decaying to jets

The time taken by a jet to reach the MTD has no significance because it consists of multiple particles with varying momenta. Therefore, in order to compute the boost factor of the LLP, we will use the timing information of the fastest charged particle from the two jets associated with a SV and assume that this particle's $\beta = 1$. This assumption introduces some error. The higher the p_T of the particle, the lower will be the corresponding error. Note also that placing higher p_T cuts makes the sample biased towards higher $\beta_T\gamma$ values.

In Fig. 15 we compare the boost factor distribution at the parton level with the one estimated using the timing of the fastest charged particle with no p_T cut and lower p_T cuts of 2 GeV and 5 GeV respectively. We find that for LLP of mass 100 GeV, if we place a cut of 2 GeV on the fastest charged particle coming from the LLP decay, the assumption of this particle's $\beta = 1$ works quite well, and we obtain a distribution from timing that is comparable to the parton-level distribution. For a LLP of mass 1000 GeV, higher p_T cuts ($p_T > 5$ GeV) work better.

Comparing Fig. 15 (centre panel) with Fig. 10, where the latter shows the comparison of the parton-level $\beta_T\gamma$ distribution − without and with EC and that calculated from final state jet information, we find that timing improves the boost factor measurement. Hence, it will also improve the lifetime estimation.

4.2.2 LLPs decays involving invisible particle

For LLPs decaying into leptons and missing particles, for both two-body and three-body decays, Figs. 16 and 17 show that the boost factor distribution obtained from timing of any one of the leptons coming from the LLP decay is comparable to the parton-level distribution.

Therefore, timing information can help us to get the boost of the LLP if we know the SV and if any one of the decay products is a charged particle with $p_T > 0.7$ GeV

mother particle's masses to great precision as shown in [71] for processes like $e^+e^- \to \tilde{\chi}_1^+\tilde{\chi}_1^- \to \tilde{\chi}_1^0\tilde{\chi}_1^0 W^+W^-$ and $e^+e^- \to \tilde{\chi}_2^0\tilde{\chi}_2^0 \to \tilde{\chi}_1^0\tilde{\chi}_1^0 ZZ$ for prompt decays [71] can be extended to long-lived scenarios, we can then reconstruct the DM ($\tilde{\chi}_1^0$) mass at ILC even for the two body decays of the LLP using Eq. (4.2).

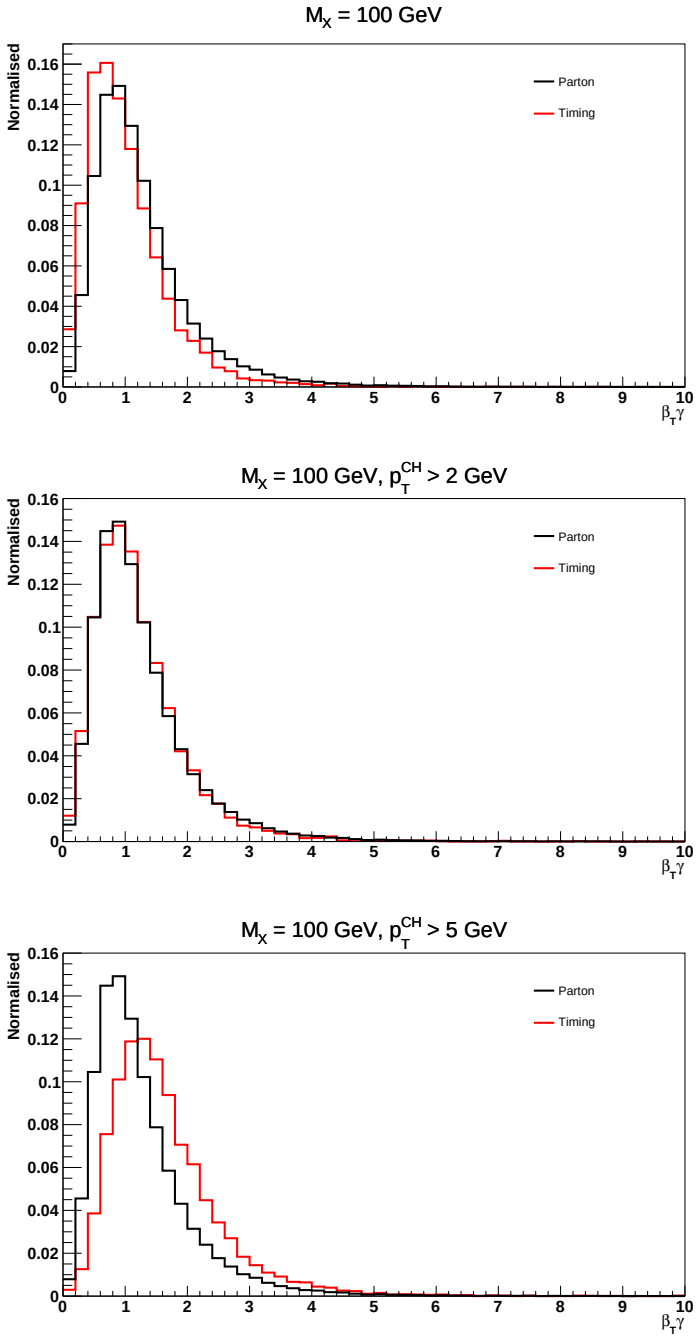

Figure 15: $\beta_T\gamma$ distribution of an LLP of mass 100 GeV at parton level and using timing information with no p_T cut (top), $p_T > 2$ GeV (centre), and $p_T > 5$ GeV (bottom) for the fastest charged hadron coming from a SV.

in the barrel and $p > 0.7$ GeV in the endcaps, even when its decay products cannot be reconstructed entirely due to presence of invisible particles. We can then apply any one of the previous discussed methods in Sec. 3.1.2 to estimate the lifetime of the LLP, especially the model-independent χ^2 analysis which crucially needs the boost

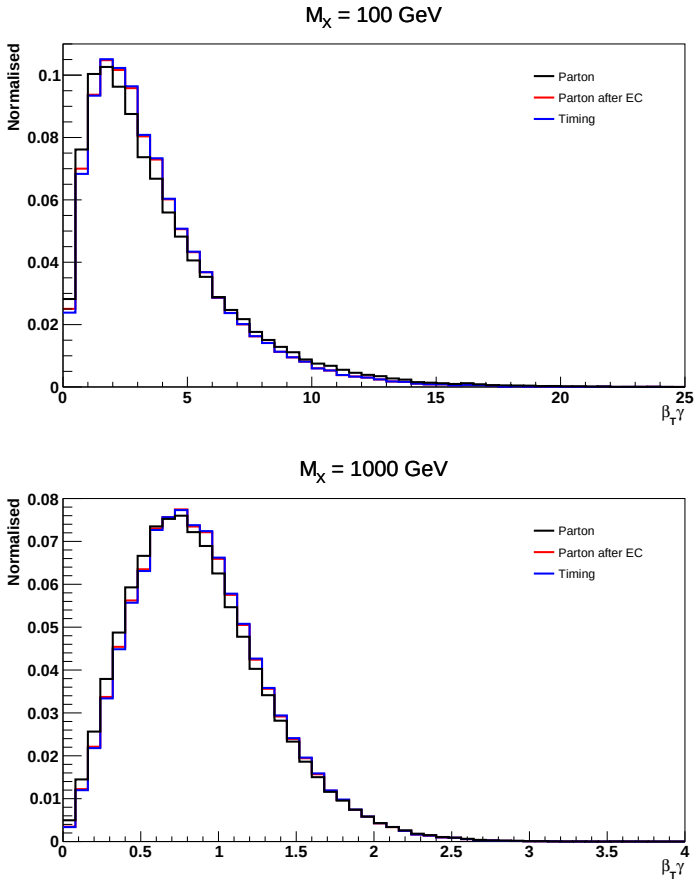

Figure 16: $\beta_T\gamma$ distribution for two-body decay of an LLP of mass 100 GeV (top) and 1000 GeV (bottom) at parton level without cuts, parton level with cuts and using timing information.

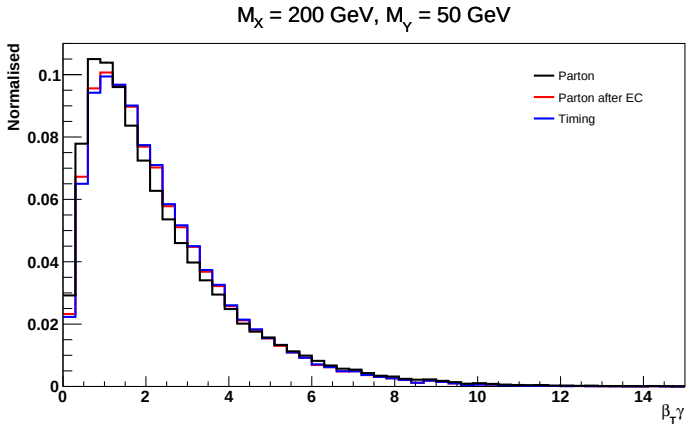

Figure 17: $\beta_T\gamma$ distribution for three-body decay of an LLP of mass 200 GeV into two muons and an invisible particle of mass 50 GeV at parton level without cuts, parton level with cuts and using timing information.

information of the LLP [10].

5 Conclusions and outlook

The goal of the present work is to study the properties of LLPs, especially their lifetimes in an optimistic scenario when such particles are discovered at the LHC or future colliders. We examined a variety of different signatures, namely decays of neutral LLPs into pairs of displaced leptons, displaced jets or displaced leptons accompanied by missing transverse energy as well as the decay of an electrically charged LLP into missing energy along with a charged SM lepton. Perhaps unsurprisingly, in all cases we found that it is, indeed, possible to reconstruct the LLP lifetime if we assume that the underlying model is known. Going a step further, however, we showed that – at least within the limitations of our study – in most cases it is also possible to estimate the LLP lifetime in a model-independent manner, provided the LLP $\beta\gamma$ distribution can be experimentally accessed. We moreover commented upon how upgrades of the LHC detectors, and in particular the improvement of timing measurements, can be used in order to facilitate the determination of different quantities entering LLP-related measurements.

The present work is a theorists analysis of a topic which heavily depends on experimental information. There are numerous ways through which our study could be improved and/or extended. For instance, other than examining different final states that we have not considered here, it is clear that our treatment of experimental limitations related, *e.g.*, to the determination of the secondary vertex location or, perhaps most crucially, to the measurement of the LLP $\beta\gamma$ distribution, can be improved. In this respect, we deem our results to be on the optimistic side. On the other side of the spectrum, nevertheless, in our analysis we mostly focused on information that can be inferred from the tracker systems of the LHC detectors. However, *e.g.* in the case of kinked track signatures, calorimetric information can be used in the framework of an offline analysis in order to identify decay events in which the SM lepton track is too short to be reconstructed, but its presence can be inferred by energy depositions in the ECAL. Our hope is that this preliminary study will trigger more detailed analyses on the topic.

Acknowledgments

We would like to thank the organizers of the 2017 "Les Houches – Physics at TeV colliders" workshop where this work was initiated. We thank Daniele Barducci for

[10] Along the same lines, we can also expect to reconstruct the lifetime of LLPs decaying to give photons in the final state using the timing information of the ECAL, which although is not very precise and has a resolution of few 100 ps [72], can still give an estimate.

collaboration during the earlier stages of this work. We thank Swagata Mukherjee and Shilpi Jain for helpful discussions. The work of B.H. and S.B. are partially supported by *Investissements d'avenir*, Labex ENIGMASS, contrat ANR-11-LABX-0012. S.B. is also supported by a Durham Junior Research Fellowship COFUNDed by Durham University and the European Union. The works of S.B. and B.B. are partially supported by the CNRS LIA-THEP (Theoretical High Energy Physics) and the INFRE-HEPNET (IndoFrench Network on High Energy Physics) of CEFIPRA/IFCPAR (Indo-French Centre for the Promotion of Advanced Research). The work of S.B. is also partially supported by a Durham Junior Research Fellowship COFUNDed between Durham University and the European Union under grant agreement number 609412. The work of B.B. is also supported by the Department of Science and Technology, Government of India, under the Grant Agreement number IFA13-PH-75 (INSPIRE Faculty Award). A.G. would like to thank the Laboratoire de Physique Théorique et Hautes Énergies, where part of this work was performed, for warm hospitality and Dimitris Varouchas for illuminating discussions. The work of D.S. is supported by the National Science Foundation under Grant No. Grant No. PHY-1915147. R.S. would like to thank Rahool Kumar Barman and Amit Adhikary for useful discussions.

References

[1] G. F. Giudice and R. Rattazzi, "Theories with gauge mediated supersymmetry breaking," *Phys. Rept.* **322** (1999) 419–499, arXiv:hep-ph/9801271 [hep-ph].

[2] G. F. Giudice and A. Romanino, "Split supersymmetry," *Nucl. Phys.* **B699** (2004) 65–89, arXiv:hep-ph/0406088 [hep-ph]. [Erratum: Nucl. Phys.B706,487(2005)].

[3] G. Burdman, Z. Chacko, H.-S. Goh, and R. Harnik, "Folded supersymmetry and the LEP paradox," *JHEP* **02** (2007) 009, arXiv:hep-ph/0609152 [hep-ph].

[4] S. Biswas and B. Mukhopadhyaya, "Neutralino reconstruction in supersymmetry with long-lived staus," *Phys. Rev.* **D79** (2009) 115009, arXiv:0902.4349 [hep-ph].

[5] P. Meade, M. Reece, and D. Shih, "Long-Lived Neutralino NLSPs," *JHEP* **10** (2010) 067, arXiv:1006.4575 [hep-ph].

[6] S. Biswas, J. Chakrabortty, and S. Roy, "Multi-photon signal in supersymmetry comprising non-pointing photon(s) at the LHC," *Phys. Rev.* **D83** (2011) 075009, arXiv:1010.0949 [hep-ph].

[7] M. Ibe, S. Matsumoto, and T. T. Yanagida, "Pure Gravity Mediation with $m_{3/2} = 10$–100 TeV," *Phys. Rev.* **D85** (2012) 095011, arXiv:1202.2253 [hep-ph].

[8] P. W. Graham, D. E. Kaplan, S. Rajendran, and P. Saraswat, "Displaced Supersymmetry," *JHEP* **07** (2012) 149, arXiv:1204.6038 [hep-ph].

[9] B. Bhattacherjee, B. Feldstein, M. Ibe, S. Matsumoto, and T. T. Yanagida, "Pure gravity mediation of supersymmetry breaking at the Large Hadron Collider," *Phys. Rev.* **D87** no. 1, (2013) 015028, arXiv:1207.5453 [hep-ph].

[10] A. Arvanitaki, N. Craig, S. Dimopoulos, and G. Villadoro, "Mini-Split," *JHEP* **02** (2013) 126, arXiv:1210.0555 [hep-ph].

[11] D. G. Cerdeo, V. Martn-Lozano, and O. Seto, "Displaced vertices and long-lived charged particles in the NMSSM with right-handed sneutrinos," *JHEP* **05** (2014) 035, arXiv:1311.7260 [hep-ph].

[12] K. Rolbiecki and K. Sakurai, "Long-lived bino and wino in supersymmetry with heavy scalars and higgsinos," *JHEP* **11** (2015) 091, arXiv:1506.08799 [hep-ph].

[13] D. Dercks, J. De Vries, H. K. Dreiner, and Z. S. Wang, "R-parity Violation and Light Neutralinos at CODEX-b, FASER, and MATHUSLA," *Phys. Rev.* **D99** no. 5, (2019) 055039, arXiv:1810.03617 [hep-ph].

[14] H. Fukuda, N. Nagata, H. Oide, H. Otono, and S. Shirai, "Cornering Higgsino: Use of Soft Displaced Track," arXiv:1910.08065 [hep-ph].

[15] Z. Chacko, H.-S. Goh, and R. Harnik, "The Twin Higgs: Natural electroweak breaking from mirror symmetry," *Phys. Rev. Lett.* **96** (2006) 231802, arXiv:hep-ph/0506256 [hep-ph].

[16] M. J. Strassler and K. M. Zurek, "Echoes of a hidden valley at hadron colliders," *Phys. Lett.* **B651** (2007) 374–379, arXiv:hep-ph/0604261 [hep-ph].

[17] M. J. Strassler and K. M. Zurek, "Discovering the Higgs through highly-displaced vertices," *Phys. Lett.* **B661** (2008) 263–267, arXiv:hep-ph/0605193 [hep-ph].

[18] M. J. Strassler, "Possible effects of a hidden valley on supersymmetric phenomenology," arXiv:hep-ph/0607160 [hep-ph].

[19] L. J. Hall, K. Jedamzik, J. March-Russell, and S. M. West, "Freeze-In Production of FIMP Dark Matter," *JHEP* **03** (2010) 080, arXiv:0911.1120 [hep-ph].

[20] D. Tucker-Smith and N. Weiner, "Inelastic dark matter," *Phys. Rev.* **D64** (2001) 043502, arXiv:hep-ph/0101138 [hep-ph].

[21] R. T. Co, F. D'Eramo, L. J. Hall, and D. Pappadopulo, "Freeze-In Dark Matter with Displaced Signatures at Colliders," *JCAP* **1512** no. 12, (2015) 024, arXiv:1506.07532 [hep-ph].

[22] A. G. Hessler, A. Ibarra, E. Molinaro, and S. Vogl, "Probing the scotogenic FIMP at the LHC," *JHEP* **01** (2017) 100, arXiv:1611.09540 [hep-ph].

[23] G. Blanger *et al.*, "LHC-friendly minimal freeze-in models," *JHEP* **02** (2019) 186, arXiv:1811.05478 [hep-ph].

[24] A. Goudelis, K. A. Mohan, and D. Sengupta, "Clockworking FIMPs," *JHEP* **10** (2018) 014, arXiv:1807.06642 [hep-ph].

[25] J. M. No, P. Tunney, and B. Zaldivar, "Probing Dark Matter freeze-in with long-lived particle signatures: MATHUSLA, HL-LHC and FCC-hh," arXiv:1908.11387 [hep-ph].

[26] Y. Cui and B. Shuve, "Probing Baryogenesis with Displaced Vertices at the LHC," *JHEP* **02** (2015) 049, arXiv:1409.6729 [hep-ph].

[27] **ATLAS** Collaboration, G. Aad *et al.*, "Search for nonpointing and delayed photons in the diphoton and missing transverse momentum final state in 8 TeV pp collisions at the LHC using the ATLAS detector," *Phys. Rev.* **D90** no. 11, (2014) 112005, arXiv:1409.5542 [hep-ex].

[28] **ATLAS** Collaboration, M. Aaboud *et al.*, "Search for long-lived charginos based on a disappearing-track signature in pp collisions at $\sqrt{s} = 13$ TeV with the ATLAS detector," arXiv:1712.02118 [hep-ex].

[29] **ATLAS** Collaboration, M. Aaboud *et al.*, "Search for long-lived, massive particles in events with displaced vertices and missing transverse momentum in $\sqrt{s} = 13$ TeV pp collisions with the ATLAS detector," arXiv:1710.04901 [hep-ex].

[30] **ATLAS** Collaboration, G. Aad *et al.*, "Search for light long-lived neutral particles produced in pp collisions at $\sqrt{s} = 13$ TeV and decaying into collimated leptons or light hadrons with the ATLAS detector," arXiv:1909.01246 [hep-ex].

[31] **ATLAS** Collaboration, M. Aaboud *et al.*, "Search for long-lived neutral particles in pp collisions at $\sqrt{s} = 13$ TeV that decay into displaced hadronic jets in the ATLAS calorimeter," *Eur. Phys. J.* **C79** no. 6, (2019) 481, arXiv:1902.03094 [hep-ex].

[32] **ATLAS** Collaboration, G. Aad *et al.*, "Search for displaced vertices of oppositely charged leptons from decays of long-lived particles in pp collisions at $\sqrt{s} = 13$ TeV with the ATLAS detector," arXiv:1907.10037 [hep-ex].

[33] **CMS** Collaboration, V. Khachatryan *et al.*, "Search for long-lived charged particles in proton-proton collisions at $\sqrt{s} = 13$TeV," *Phys. Rev.* **D94** no. 11, (2016) 112004, arXiv:1609.08382 [hep-ex].

[34] **CMS** Collaboration, A. M. Sirunyan *et al.*, "Search for new long-lived particles at $\sqrt{s} = 13$ TeV," arXiv:1711.09120 [hep-ex].

[35] **CMS** Collaboration, A. M. Sirunyan *et al.*, "Search for decays of stopped exotic long-lived particles produced in proton-proton collisions at $\sqrt{s} = 13$ TeV," arXiv:1801.00359 [hep-ex].

[36] **CMS** Collaboration, A. M. Sirunyan *et al.*, "Search for long-lived particles using nonprompt jets and missing transverse momentum with proton-proton collisions at $\sqrt{s} = 13$ TeV," *Phys. Lett.* **B797** (2019) 134876, arXiv:1906.06441 [hep-ex].

[37] **CMS** Collaboration, A. M. Sirunyan *et al.*, "Search for long-lived particles using delayed photons in proton-proton collisions at $\sqrt{s} = 13$ TeV," *Phys. Rev.* **D100** no. 11, (2019) 112003, arXiv:1909.06166 [hep-ex].

[38] J. Alimena *et al.*, "Searching for Long-Lived Particles beyond the Standard Model at the Large Hadron Collider," arXiv:1903.04497 [hep-ex].

[39] **FASER** Collaboration, A. Ariga *et al.*, "FASER: ForwArd Search ExpeRiment at the LHC," arXiv:1901.04468 [hep-ex].

[40] **MATHUSLA** Collaboration, H. Lubatti *et al.*, "MATHUSLA: A Detector Proposal to Explore the Lifetime Frontier at the HL-LHC," 2019. arXiv:1901.04040 [hep-ex]. http://mathusla.web.cern.ch.

[41] J. L. Feng, I. Galon, F. Kling, and S. Trojanowski, "ForwArd Search ExpeRiment at the LHC," *Phys. Rev.* **D97** no. 3, (2018) 035001, arXiv:1708.09389 [hep-ph].

[42] J. P. Chou, D. Curtin, and H. J. Lubatti, "New Detectors to Explore the Lifetime Frontier," *Phys. Lett.* **B767** (2017) 29–36, arXiv:1606.06298 [hep-ph].

[43] D. Curtin *et al.*, "Long-Lived Particles at the Energy Frontier: The MATHUSLA Physics Case," arXiv:1806.07396 [hep-ph].

[44] M. Kawasaki, K. Kohri, T. Moroi, and Y. Takaesu, "Revisiting Big-Bang Nucleosynthesis Constraints on Long-Lived Decaying Particles," *Phys. Rev.* **D97** no. 2, (2018) 023502, arXiv:1709.01211 [hep-ph].

[45] G. Brooijmans *et al.*, "Les Houches 2017: Physics at TeV Colliders New Physics Working Group Report," in *Les Houches 2017: Physics at TeV Colliders New Physics Working Group Report*. 2018. arXiv:1803.10379 [hep-ph]. http://lss.fnal.gov/archive/2017/conf/fermilab-conf-17-664-ppd.pdf.

[46] S. Asai, K. Hamaguchi, and S. Shirai, "Measuring lifetimes of long-lived charged massive particles stopped in LHC detectors," *Phys. Rev. Lett.* **103** (2009) 141803, arXiv:0902.3754 [hep-ph].

[47] S. Ambrosanio, B. Mele, A. Nisati, S. Petrarca, G. Polesello, A. Rimoldi, and G. Salvini, "SUSY longlived massive particles: Detection and physics at the LHC," *Rend. Lincei Sci. Fis. Nat.* **12** (2001) 5–18, arXiv:hep-ph/0012192 [hep-ph].

[48] R. Barbier *et al.*, "R-parity violating supersymmetry," *Phys. Rept.* **420** (2005) 1–202, arXiv:hep-ph/0406039 [hep-ph].

[49] T. Sjostrand, S. Mrenna, and P. Z. Skands, "PYTHIA 6.4 Physics and Manual," *JHEP* **05** (2006) 026, arXiv:hep-ph/0603175 [hep-ph].

[50] A. Collaboration, "Technical Design Report for the ATLAS Inner Tracker Pixel Detector," Tech. Rep. CERN-LHCC-2017-021. ATLAS-TDR-030, CERN, Geneva, Sep, 2017. https://cds.cern.ch/record/2285585.

[51] **ATLAS Collaboration** Collaboration, "Performance of vertex reconstruction algorithms for detection of new long-lived particle decays within the ATLAS inner detector," Tech. Rep. ATL-PHYS-PUB-2019-013, CERN, Geneva, Mar, 2019. https://cds.cern.ch/record/2669425.

[52] **CMS** Collaboration, S. Chatrchyan *et al.*, "Description and performance of track

and primary-vertex reconstruction with the CMS tracker," *JINST* **9** no. 10, (2014) P10009, arXiv:1405.6569 [physics.ins-det].

[53] **ATLAS** Collaboration, M. Aaboud *et al.*, "Search for long-lived particles in final states with displaced dimuon vertices in pp collisions at $\sqrt{s} = 13$ TeV with the ATLAS detector," *Phys. Rev.* **D99** no. 1, (2019) 012001, arXiv:1808.03057 [hep-ex].

[54] **CMS Collaboration** Collaboration, M. Backhaus, "The Upgrade of the CMS Inner Tracker for HL-LHC," Tech. Rep. CMS-CR-2019-011, CERN, Geneva, Feb, 2019. https://cds.cern.ch/record/2683265.

[55] R. Brun and F. Rademakers, "ROOT: An object oriented data analysis framework," *Nucl. Instrum. Meth.* **A389** (1997) 81–86.

[56] G. Cowan, *Statistical Data Analysis*. Clarendon Press, Oxford, 1998.

[57] A. J. Barr, "Measuring slepton spin at the LHC," *JHEP* **02** (2006) 042, arXiv:hep-ph/0511115 [hep-ph].

[58] **ATLAS** Collaboration, G. Aad *et al.*, "Evidence for the spin-0 nature of the Higgs boson using ATLAS data," *Phys. Lett.* **B726** (2013) 120–144, arXiv:1307.1432 [hep-ex].

[59] **CMS** Collaboration, V. Khachatryan *et al.*, "Constraints on the spin-parity and anomalous HVV couplings of the Higgs boson in proton collisions at 7 and 8 TeV," *Phys. Rev.* **D92** no. 1, (2015) 012004, arXiv:1411.3441 [hep-ex].

[60] S. Banerjee, G. Blanger, B. Bhattacherjee, F. Boudjema, R. M. Godbole, and S. Mukherjee, "Novel signatures for long-lived particles at the LHC," arXiv:1706.07407 [hep-ph].

[61] B. Bhattacherjee, S. Mukherjee, and R. Sengupta, "Study of energy deposition patterns in hadron calorimeter for prompt and displaced jets using convolutional neural network," *JHEP* **11** (2019) 156, arXiv:1904.04811 [hep-ph].

[62] W. S. Cho, K. Choi, Y. G. Kim, and C. B. Park, "Gluino Stransverse Mass," *Phys. Rev. Lett.* **100** (2008) 171801, arXiv:0709.0288 [hep-ph].

[63] J. A. Evans and J. Shelton, "Long-Lived Staus and Displaced Leptons at the LHC," *JHEP* **04** (2016) 056, arXiv:1601.01326 [hep-ph].

[64] **ATLAS Collaboration** Collaboration, "Performance of tracking and vertexing techniques for a disappearing track plus soft track signature with the ATLAS detector," Tech. Rep. ATL-PHYS-PUB-2019-011, CERN, Geneva, Mar, 2019. https://cds.cern.ch/record/2669015.

[65] **ATLAS Collaboration** Collaboration, "Performance of the reconstruction of large impact parameter tracks in the ATLAS inner detector," Tech. Rep. ATL-PHYS-PUB-2017-014, CERN, Geneva, Jul, 2017. https://cds.cern.ch/record/2275635.

[66] C. Collaboration, "Technical Proposal for a Mip Timing Detector in the CMS Experiment Phase 2 Upgrade,". https://cds.cern.ch/record/2296612. Technical Report No. CERN-LHCC-2017-027, LHCC-P-009, CERN, Geneva.

[67] J. Liu, Z. Liu, and L.-T. Wang, "Enhancing Long-Lived Particles Searches at the LHC with Precision Timing Information," *Phys. Rev. Lett.* **122** no. 13, (2019) 131801, arXiv:1805.05957 [hep-ph].

[68] J. D. Mason, "Time-Delayed Electrons from Higgs Decays to Right-Handed Neutrinos," *JHEP* **07** (2019) 089, arXiv:1905.07772 [hep-ph].

[69] Z. Flowers, D. W. Kang, Q. Meier, S. C. Park, and C. Rogan, "Timing information at HL-LHC: Complete determination of masses of Dark Matter and Long lived particle," arXiv:1903.05825 [hep-ph].

[70] **DELPHES 3** Collaboration, J. de Favereau, C. Delaere, P. Demin, A. Giammanco, V. Lematre, A. Mertens, and M. Selvaggi, "DELPHES 3, A modular framework for fast simulation of a generic collider experiment," *JHEP* **02** (2014) 057, arXiv:1307.6346 [hep-ex].

[71] Y. Li and A. Nomerotski, "Chargino and Neutralino Masses at ILC," in *International Linear Collider Workshop (LCWS10 and ILC10) Beijing, China, March 26-30, 2010*. 2010. arXiv:1007.0698 [physics.ins-det].

[72] **CMS** Collaboration, C. Collaboration, "Search for long-lived neutral particles in the final state of delayed photons and missing energy in proton-proton collisions at $\sqrt{s}$ = 8 TeV,".